# *Molecular characterization and distribution of the voltage-gated sodium channel, Para, in the brain of the grasshopper and vinegar fly*

**Hongxia Wang, Bert Foquet, Richard B. Dewell, Hojun Song, Herman A. Dierick & Fabrizio Gabbiani**


**Journal of Comparative Physiology A**
Neuroethology, Sensory, Neural, and Behavioral Physiology

ISSN 0340-7594

J Comp Physiol A
DOI 10.1007/s00359-019-01396-4

Springer

Journal of Comparative Physiology A
https://doi.org/10.1007/s00359-019-01396-4

ORIGINAL PAPER

# Molecular characterization and distribution of the voltage-gated sodium channel, Para, in the brain of the grasshopper and vinegar fly

**Hongxia Wang[1] · Bert Foquet[2] · Richard B. Dewell[1] · Hojun Song[2] · Herman A. Dierick[1,3] · Fabrizio Gabbiani[1,4]**

Received: 22 August 2019 / Revised: 10 December 2019 / Accepted: 14 December 2019


## Abstract

Voltage-gated sodium (NaV) channels, encoded by the gene *para*, play a critical role in the rapid processing and propagation of visual information related to collision avoidance behaviors. We investigated their localization by immunostaining the optic lobes and central brain of the grasshopper *Schistocerca americana* and the vinegar fly *Drosophila melanogaster* with an antibody that recognizes the channel peptide domain responsible for fast inactivation gating. NaV channels were detected at high density at all stages of development. In the optic lobe, they revealed stereotypically repeating fascicles consistent with the regular structure of the eye. In the central brain, major axonal tracts were strongly labeled, particularly in the grasshopper olfactory system. We used the NaV channel sequence of *Drosophila* to identify an ortholog in the transcriptome of *Schistocerca*. The grasshopper, vinegar fly, and human NaV channels exhibit a high degree of conservation at gating and ion selectivity domains. Comparison with three species evolutionarily close to *Schistocerca* identified splice variants of Para and their relation to those of *Drosophila*. The anatomical distribution of NaV channels molecularly analogous to those of humans in grasshoppers and vinegar flies provides a substrate for rapid signal propagation and visual processing in the context of visually-guided collision avoidance.

**Keywords** *Drosophila* · *Schistocerca* · Pan-Nav · Para · Optic lobe

## Introduction

A hallmark of visual processing in insects is its speed. In part, this rapidity relies on graded potential neurons. For example, large monopolar cells in the lamina perform center-surround and temporal filtering on photoreceptor signals using graded potentials (Srinivasan et al. 1982; van Hateren 1992); tangential cells in the lobula plate of dipteran flies extract behaviorally relevant optic flow parameters mostly using graded potentials (Krapp and Hengstenberg 1996; Cuntz et al. 2003). However, when urgent reactions requiring rapid long-distance propagation of information are warranted, for instance in life threatening situations such as collision avoidance with a potential predator, they are invariably activated by spiking neurons (Fotowat et al. 2011; de Vries and Clandinin 2012; von Reyn et al. 2014). Collision avoidance has been extensively studied in grasshoppers and vinegar flies (Fotowat and Gabbiani 2011; Peek and Card 2016). In grasshoppers, two identified neurons, the lobula giant movement detector (LGMD) in the optic lobe and its postsynaptic partner the descending contralateral movement detector (DCMD) in the central brain convey

Hojun Song, Herman A. Dierick and Fabrizio Gabbiani contributed equally to this work.

Hongxia Wang, Bert Foquet and Richard B. Dewell are the co-first authors.

**Electronic supplementary material** The online version of this article (https://doi.org/10.1007/s00359-019-01396-4) contains supplementary material, which is available to authorized users.

✉ Fabrizio Gabbiani
gabbiani@bcm.edu

[1] Department of Neuroscience, Baylor College of Medicine, Houston, USA

[2] Department of Entomology, Texas A&M University, College Station, USA

[3] Department of Molecular and Human Genetics, Baylor College of Medicine, Houston, USA

[4] Department of Electrical and Computer Engineering, Rice University, Houston, USA

Published online: 04 January 2020

visual information about impending collision through their spiking activity starting from the earliest developmental stages (Simmons et al. 2013; Sztarker and Rind 2014). Yet, little is known about the localization and distribution of spike-generating NaV channels in the visual neuropils of grasshoppers, vinegar flies or other insects and, more broadly, in their central brain. In insects, most NaV channels are encoded by a single gene *para* (Dong et al. 2014), which in *Drosophila* generates more than sixty isoforms through alternative splicing and RNA editing (Loughney et al. 1989; Thackeray and Ganetzky 1994). Two different polyclonal antibodies have been previously developed against *Drosophila* Para, but neither of them convincingly revealed its specific localization (Amichot et al. 1993; Xiao et al. 2017). Reliable, spatially resolved antibody staining is of particular interest for grasshoppers and other non-genetic insect models. For them, there are no alternative genetic techniques to map protein expression, such as protein traps (Venken et al. 2011). Because NaV channels are highly conserved across the animal kingdom (Moran et al. 2015), we reasoned that an antibody against vertebrate NaV channels might reveal their localization in the optic lobe and central brain of the grasshopper and vinegar fly. We thus used a mouse monoclonal pan-Nav antibody known to broadly stain for NaV channels in the mammalian brain (Rasband et al. 1999). The robust immune-staining pattern of NaV channels observed in the grasshopper and vinegar fly brain prompted us to search for an ortholog of the *Drosophila* Para protein in grasshoppers. By analyzing RNA sequencing (RNA-seq) data from the thorax and head of the grasshopper *Schistocerca americana* using one of the *Drosophila* Para isoforms, we assembled a full-length sequence. We compared this sequence to human Nav1.1, to the *Drosophila* Para protein isoforms, and to sequences from three more closely related Polyneopteran species, the German cockroach, the drywood and dampwood termites.

## Materials and methods

### Animals

We used the grasshopper *Schistocerca americana*, a common species found in the southeastern United States (Kuitert and Connin 1952). Grasshoppers are hemimetabolous insects developing through several nymphal instars (stages) that are similar to their adult form except for the lack of wings and reproductive organs (Supp. Fig. 1a). This contrasts with the development of holometaboulous insects such as *Drosophila* that pass through several larval instars and a pupal stage prior to reaching adulthood (Supp. Fig. 1b). *S. americana* individuals used for immunostaining were taken from a crowded colony maintained at Baylor College of Medicine under a 12 h light/dark cycle (32/25 ºC). They originated from individuals collected near Gainesville, Alachua County, Florida, in November 2002. They were fed wheat grass and oat bran three times per week. *S. americana* individuals used for transcriptome sequencing were from a colony maintained at Texas A&M University under a 12 h light/dark cycle at 30 ºC. They originated from a population collected in Brooksville, Pasco County, Florida, in September 2010. Individuals were reared under isolated and crowded conditions as described in Gotham and Song (2013) for an unrelated project on density-dependent phenotypic plasticity (unpublished data). Wild-type *Drosophila melanogaster* were a laboratory stock of Canton S flies. GMR42F06 flies (Pfeiffer et al. 2008) expressing GAL4 in medulla/lobula T4/T5 neurons of the optic lobe were obtained from the Bloomington Drosophila Stock Center (BL#54203) and crossed to a strain expressing GFP from a 10× UAS promoter (Pfeiffer et al. 2012; a gift from Dr. K. Venken, Baylor College of Medicine). All flies were reared on yeast, cornmeal, molasses, and agar food at room temperature ($22.5 \pm 0.5°$) on a 16-hr light/8-hr dark cycle.

### Antibodies

The specific monoclonal mouse pan-Nav antibody was generated against a synthetic peptide containing the sequence TEEQKKYYNAMKKLGSKK, which corresponds to a highly conserved segment of the intracellular III–IV loop of vertebrate sodium channels (Rasband et al. 1999), and is available from Sigma (Catalog # S8809). For 5-HT (serotonin) staining we used a whole antiserum antibody produced in rabbits (Sigma-Aldrich, Catalog # S5545) and for GFP staining a rabbit polyclonal antibody (Invitrogen, Catalog # A11122).

The specificity of the pan-Nav antibody has been verified according to several criteria. First, it labels axon initial segments and nodes of Ranvier along myelinated axons of vertebrates, sites that are known to be enriched in $Na^+$ channels (see e.g., Rasband et al. 1999; Hedstrom et al. 2007). Second, the pan-Nav antibody recognizes a protein of the correct molecular weight by immunoblot. Third and most importantly, silencing expression of $Na^+$ channels in hippocampal neurons using a pan-Nav shRNA construct eliminates all immunoreactivity in the targeted cells (Hedstrom et al. 2007, Fig. 1e). These criteria are consistent with accepted standards for the validation of antibodies in nervous system tissues (Rhodes and Trimmer 2006). For additional examples of controls using this antibody, see references available at www.antibodyregistry.org (Antibody No. AB_477552).

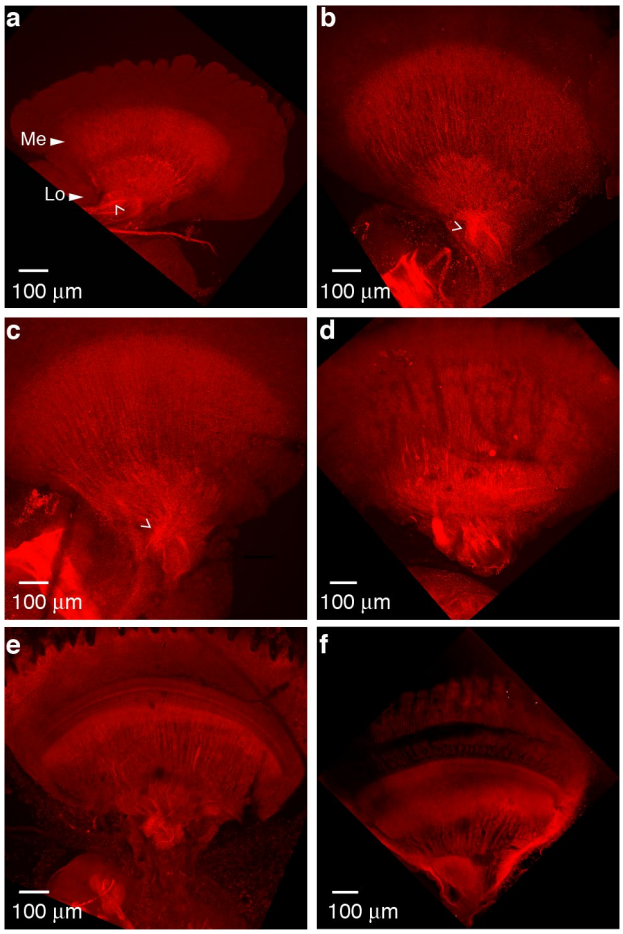


**Fig. 1** Pan-Nav protein expression pattern in the optic lobe of grasshoppers. Expression in the optic lobe of a 1st instar (**a**), 2nd instar (**b**), 3rd instar (**c**), 4th instar (**d**), 5th instar (**e**) and an adult (**f**). *Me* Medulla, *Lo* Lobula. In **a**–**c** '>' indicates axonal fibers going from the lobula of the optic lobe to the central brain. Scale bar: 100 µm (**a**–**f**)

## Immunostaining

*Schistocerca americana* has five nymphal instars (Capinera 1993). We selected individuals at all developmental stages for staining with the pan-Nav antibody. Grasshoppers were immobilized and fixed to a plastic holder for dissection of the brain and optic lobes. During the dissection, the whole head was bathed in ice-cold saline. After dissection, the brains of first to fifth instar grasshoppers were initially fixed in freshly made 4% paraformaldehyde (PFA, Electron Microscopy Science, Catalog # 15710) for one hour. Subsequently, we used shorter fixation times for fourth and fifth instar grasshoppers to improve staining results, as described in the next section. The tissues were then washed six times for 20 min using 1 × phosphate buffer solution (PBS, 0.01 M $PO_4^{3-}$; made from 10 × PBS, Thermo Fisher Scientific, catalog # Am9624) containing 0.5% Triton X-100 to promote penetration of the antibodies (Sigma-Aldrich, Catalog # 93443). Next, goat serum was added to block non-specific antigens (final concentration: 5%; Thermo Fisher Scientific, Catalog # 16210064) and tissues were incubated for one hour. Antibodies were diluted in the same solution. The pan-Nav antibody was incubated with the tissues for 48 h at a dilution of 1:350–1:800 followed by regular washing (six times, as above). Goat anti-mouse tagged with Alexa Fluor 594 was used as secondary antibody at a dilution of 1:1000 (Thermo Fisher Scientific, Catalog # A21125). Tissues were incubated with this secondary antibody for 48 h at 4 ºC followed by regular washing. To further reduce non-specific binding, the tissues were washed for another 48 h. Finally, the tissues were mounted on a glass slide, cover-slipped and sealed with nail polish.

For adult grasshoppers, the brain and optic lobes were initially fixed overnight in ice cold, freshly made 4% PFA. Subsequently, we used shorter fixation times to improve the staining results, see next section. The tissues were then washed in 10 × PBS (0.1 M $PO_4^{3-}$) for 10 min. To increase antibody penetration, adult tissues were incubated in 1 mg/ml collagenase (Sigma-Aldrich, Catalog # 10269638001) diluted in 5 × PBS. For permeabilization of cell membranes and blocking, we used 1 × PBS with 0.3% Triton X-100 and 5% goat serum in solution (PBTGS) overnight at 4 ºC. After washing out the PBTGS solution, the primary antibodies (either pan-Nav or 5-HT) were added diluted in PBTGS (1:350–1:800 pan-Nav; 1:5000 5-HT), leaving them for 4–5 days at 4 ºC. The primary antibody was washed off three times with PBTGS (20 min, 20 min, and 1 h washes; 5 min between washes). The secondary antibodies were added in PBTGS (1:1000 Alexa Fluor goat anti-mouse IgG1 for pan-Nav; 1:500 chick anti-rabbit tagged with Alexa Fluor 488 for 5-HT, Thermo Fisher Scientific, catalog # A21441) for 3 days at 4 ºC. Secondary antibodies were washed off three times in PBTGS, followed by 10 × PBS and 5 × PBS (5 min between washes). The tissue was dehydrated in an ascending ethanol series (25, 50, 75, 90, 95, 100%, 15 min each), cleared in methyl salicylate (20 min; Sigma-Aldrich, catalog # M6752), embedded in Permount (Fisher Scientific, catalog # SP15-100) and cover-slipped on a slide with a concave well (3 mm thick, 16 mm in diameter concavity, 0.8 mm deep, United Scientific Supplies, Catalog # CSTK02).

For *Drosophila*, we used adult brains and ventral nerve cords, as well 3rd instar larvae. In our initial protocol, adults were anesthetized on ice, then dissected and fixed in freshly made 4% PFA for one hour. The brains were subsequently washed and stained as described above for the grasshopper nymphal instars following established protocols for *Drosophila* (Wu and Luo 2006). *Drosophila* brains were mounted as previously described (Gnerer et al. 2015) in SlowFade Gold antifade reagent (Molecular Probes Life Technologies, Catalog # S36937).

## Additional immunostaining protocols

In rats and mice, it has been observed that staining with pan-Nav yields better results with short formaldehyde fixation times, presumably because the six lysines present in the antigen make the protocol highly sensitive to this parameter (personal communication, Dr. M. Rasband; Dapson 2007). In grasshoppers, we thus tried shorter fixation times of 10, 30 or 60 min in 4% fresh PFA at 4 ºC. The protocol was otherwise identical to that described above. Additionally, the optic lobes were cryo-sectioned at a thickness of 10–25 µm and the sections were transferred onto coverslips for antibody staining following the protocol described in (Rasband et al. 1999). Briefly, primary and secondary antibody staining lasted 60 min at room temperature, separated by three washes (5–10 min) in PBTGS. The antibody concentrations were identical to those reported above. In another variant, we embedded the optic lobe in agar at 42 ºC and sectioned it at a thickness of 200 µm after hardening. We then followed the protocol described above for the brain and optic lobes of first to fifth instar grasshoppers. In another variant, we incubated the whole tissue in 0.5% saponin either with or without collagenase in goat serum for increasing penetration and blocking non-specific binding, respectively (see above). The final variant used 0.1% saponin (Sigma-Aldrich, Catalog # 558255) and 0.5% Triton-X added to the washing solution used after tissue fixation. For the same reason, we tried 1, 2, 5, 10, and 15 min fixation times in *Drosophila*, with the protocol otherwise identical to that described above. We obtained the best results with short fixations times of 5 min in *Drosophila* and 10 min in grasshopper. It is likely that these short fixation times led to under fixation of the tissue (Dapson 2007; Ramos-Vara and Miller 2014; see "Discussion").

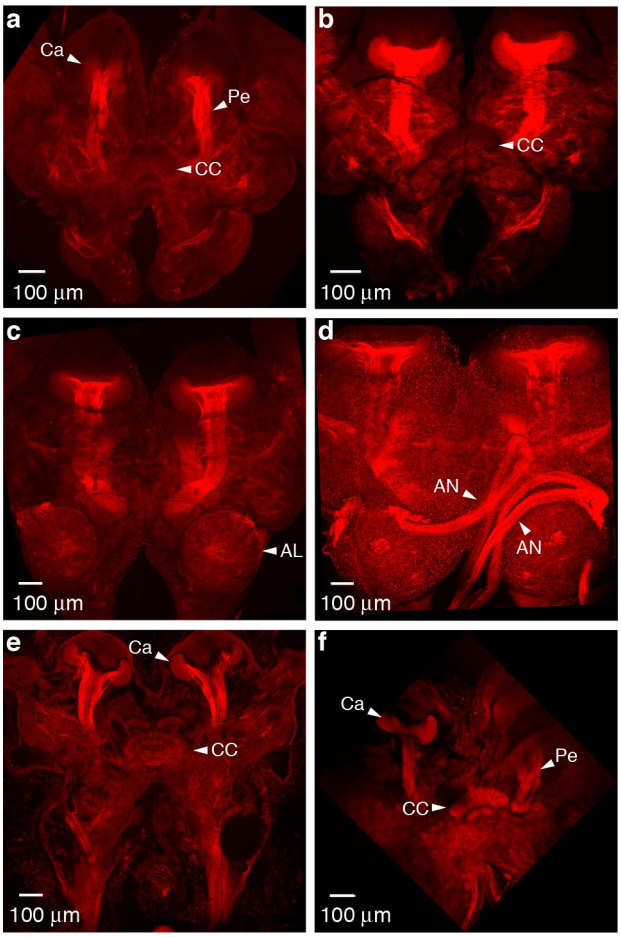


**Fig. 2** Pan-Nav protein expression pattern in the central brain of grasshoppers. Expression in the central brain of a 1st instar (**a**), 2nd instar (**b**), 3rd instar (**c**), 4th instar (**d**), 5th instar (**e**) and an adult (**f**). *Ca* calyx of the mushroom body, *Pe* peduncle of the mushroom body, *CC* central complex, *AL* antennal lobe, *AN* antennal nerve. Scale bar: 100 µm (**a**–**f**)

## Imaging

The brains and the optic lobes were typically imaged under an upright microscope with 10×, 20×, or 40× objectives using a structured illumination module (Zeiss Plan-Neofluar-10×/0.3, Plan-Neofluar-20×/0.5, Plan-Neofluar-40×/0.75, ApoTome and ZEN software). In two cases, Figs. 1f and 2f, we used a custom built two-photon microscope with a 10×/0.30 W Nikon Plan Fluor objective (Zhu and Gabbiani 2018). To image the Alexa 488 and 594 fluorescent dyes we used EGFP and Texas Red filter sets (Kramer Scientific, Catalog # KSC 295-833 and KSC 295-818). The characteristics of the excitation, dichroic and emission filters for EGFP and Texas Red can be found on the Chroma Technology web site (EGFP parts # HQ480/40X, 505DCXT, and HQ510LP; Tx Red parts # ET560/40X, T585LP, and ET630/75 M, respectively). The orientation of the preparation was optimized for imaging purposes; the resulting micrographs were rotated post acquisition to standardize their orientation and the figure background was filled with black pixels, resulting in the occasional presence of sharp oblique edges (e.g., Fig. 1a). The images shown in Figs. 1, 2 and 3 and Supp. Fig. 2, 3 and 4 are maximum intensity projections from ~ 10 to ~ 60 slices through the optic lobe or whole brain of the animal. To generate images of the fly optic lobe from a perspective showing the lobula and lobula plate (Supp. Fig. 4f), image stacks were imported into Vaa3D and rotated using the Neuron Annotator mode (Peng et al. 2010). After manual orientation, images were exported as TIFF format screenshots (see also Wu et al. 2016). Movies were assembled from stacks of images acquired with the following resolutions ($x$, $y$ and $z$): $0.650 \times 0.650 \times 4.55$ µm (Supp. Movie 1), $0.325 \times 0.325 \times 1.35$ µm (Supp. Movies 2, 5), or $0.163 \times 0.163 \times 0.600$ µm (Supp. Movies 3, 4).

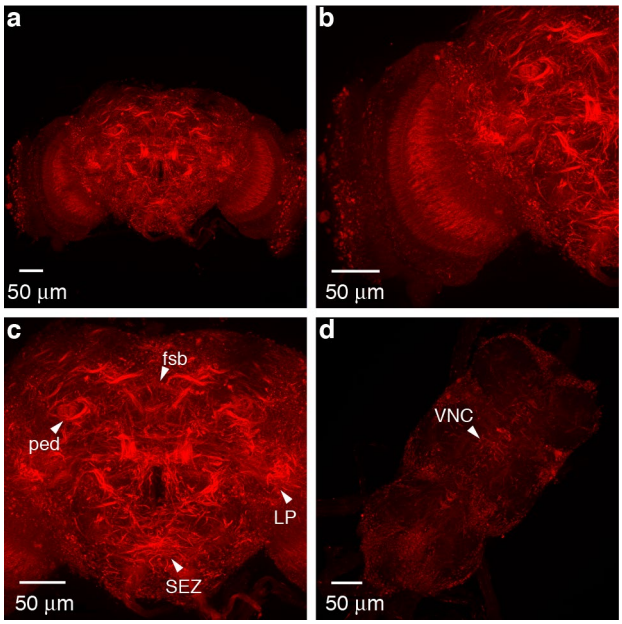


**Fig. 3** Pan-Nav protein expression pattern in the brain and ventral nerve cord (VNC) of adult *Drosophila*. **a** Whole brain image of an adult *Drosophila*. **b** Close-up of the optic lobe. **c** Close-up image of the central brain. **d** Image of the adult VNC. In **a**–**d** fixation time was 5 min. In **c**, **d** arrowheads show representative fascicles in resolved brain areas. *ped* peduncle of the mushroom body, *LP* lateral protocerebrum, *SEZ* sub esophageal zone, *fsb* fan-shaped body, *VNC* ventral nerve cord. Scale bar: 50 µm (**a**–**d**)

## Annotation

To identify brain structures we consulted, respectively, the brain atlas of *Schistocerca gregaria*, a species closely related to *Schistocerca americana*, and that of *Drosophila* (Strausfeld 1976; Kurylas et al. 2008; El Jundi et al. 2010; Ito et al. 2014).

## Sequencing grasshopper thorax and head RNA

To standardize the developmental stage specimens, we used last nymphal instar females that molted in the morning. They were dissected between 8 and 9 AM, roughly 72 h after molting. We preserved head and thorax tissues at −20 °C in RNAlater (Qiagen, Valencia, CA). A total of ten specimens, five isolated and five crowded individuals, were dissected. RNA was extracted using a Trizol-chloroform isolation protocol, followed by clean-up with a RNeasy mini kit, both following manufacturer's guidelines (Thermo Fisher Scientific, Waltham, MA and Qiagen, Valencia, CA, respectively). RNA purity was quantified using a spectrophotometer (DS-11, DeNovix, Wilmington, DE). Specifically, RNA extracts were used for sequencing if the ratios of 260–280 nm and of 260–230 nm absorbance values were above 2 (Imbeaud et al. 2005). Additionally, RNA integrity was analyzed by microcapillary electrophoresis with a Fragment Analyzer and ProSize software (Agilent Technologies, Ankeny, IA). RNA Quality Number (RQN) values over 3.9 were used for RNA-sequencing. This cutoff is lower than what is used in mammalian samples (Escobar and Hunt 2017). However, RQN values can vary widely across insect species due to differences in 28S ribosomal RNA structure compared to other eukaryotic species (Winnebeck et al. 2010; Macharia et al. 2015; Fabrick and Hull 2017, personal communication, Assessing integrity of insect RNA, Agilent Application Note). The samples were processed as part of a larger RNA-seq study of density-dependent phenotypic plasticity in *Schistocerca*, which generated a total of 80 sequenced samples. We used Illumina's TruSeq Stranded Total RNA Library Prep Kit for library preparation and performed paired-end sequencing (150 bp) using 8.5 lanes on an Illumina HiSeq4000 (San Diego, CA). The library preparation and sequencing were performed at Texas A&M's AgriLife Research Genomics and Bioinformatics Service. Sequence cluster identification, quality prefiltering, base calling and uncertainty assessment were all done in real time at the genomics core using Illumina's software (HCS 2.2.68; RTA 1.18.66.3; default parameter settings). Demultiplexing base call files and formatting them into FASTQ files was carried out using Illumina's bcl2fastq script (version 2.17.1.14).

## Post-sequencing processing

For further processing, raw reads were imported into a personalized Galaxy environment (Afgan et al. 2018) on a supercomputing cluster of the High-Performance Research Computing group of Texas A&M University (Ada, https://hprc.tamu.edu). Reads were transformed to Sanger format using FastQ Groomer (Blankenberg et al. 2010) and were subsequently filtered with Trimmomatic (Bolger et al. 2014). The filtering consisted of cutting off any bases at both ends if their quality score was lower than 30, trimming with a sliding window of 3 bases and a minimum average quality score of 30, and finally discarding all reads of less than 30 bp. Additionally, FastQ Screen (Wingett and Andrews 2018) was used to filter out reads from bacterial and other contaminating sources.

## Transcriptome assembly

The filtered reads were used for transcriptome assembly using Trinity (Grabherr et al. 2011; default settings, in silico normalization enabled). Transcriptomes were assembled separately for head and thorax tissue. Similar contigs were removed using CD-hit-EST with a threshold of 0.9 (Li and Godzik 2006; Fu et al. 2012). Finally, an extra filtering step was performed with Transrate (Smith-Unna et al. 2016), and any contig scoring below the suggested cutoff-score was

filtered out. The final transcriptomes had a total of 342,815 and 305,904 sequences for head and thorax, respectively. Trinitystats (Grabherr et al. 2011) was used to calculate the guanine-cytosine (GC) content (40.86% and 41.17% for head and thorax, respectively) and the contig N50 (597 and 622, respectively). The fraction of reads used for transcriptome assembly that mapped back to the transcriptome was assessed using bowtie2 (Langmead et al. 2009; Langmead and Salzberg 2012). We used the preset mode 'very sensitive, end-to-end' and flagstat (Li et al. 2009; Li 2011a, b; see also SAMtools manual page, available at htslib.org). The fraction of reads mapped back to the head and thorax transcriptomes was 89 and 85.2%, respectively. Lastly, the completeness of the transcriptome was assessed with BUSCO (Benchmarking Universal Single-Copy Orthologs; Simão et al. 2015) by looking for single-copy orthologs of the lineage Insecta. For both transcriptomes the amount of complete BUSCOs was over 96% and the amount of single-copy BUSCOs in both transcriptomes was over 80%.

### *Schistocerca americana* Para sequence assembly

The assembled transcriptome sequences were imported into Geneious (R10.2.6; BioMatters, Ltd., Auckland, New Zealand). We searched for the *para* gene in the *S. americana* transcriptome data using as reference different isoforms of the paralytic locus (*para*) of *Drosophila melanogaster* with the program Megablast (*E* value $10^{-5}$, word size of 28, scoring of, respectively, 1 and −2 for Match and Mismatch, and low complexity filter on). The resulting partial sequences were manually combined and curated based on the orthologs in *D. melanogaster* and the cockroach, *B. germanica*. Where needed, sequence information was inferred from three closely related grasshopper species that were sequenced in the same RNA sequencing project (*S. serialis cubense*, *S. piceifrons*, *S. nitens*, unpublished data; https://orthoptera.speciesfile.org). Raw reads for each specimen were mapped back to the full transcriptome in Galaxy using bowtie2 (very sensitive end-to-end, disable no-mixed and no-discordant behavior). Mapping statistics were assessed using SAMtools' idxstats (Li et al. 2009). Transcript expression levels were calculated using the Transcripts per Million (TPM) normalization method in R (version 3.5.2; www.r-project.org). Because the sequence from exons 1 to 17 was fragmented into several small pieces, the comparison of transcript levels between head and thorax was based on the sequence from exon 18 to 31.

### Multiple sequence alignment and splice form characterization

We performed sequence alignments between human Nav1.1 and different insect Para sequences using the software program SnapGene (GSL Biotech; available at snapgene.com). The transmembrane domains and pore forming domains delimited by light blue boxes in Figs. 4 and 5, where obtained from the annotation of the Human SCN1A protein (Nav1.1) in Uniprot (www.uniprot.org, P35498). The corresponding domains in the *D. melanogaster* Para protein often differ by a few amino acids at each of their ends (P35500). We used the FlyBase listing of *Drosophila* Para isoforms to construct an exon/intron map of the *para* locus. To assess whether other splice forms exist in *Schistocerca*, we mined our transcriptome data using the reconstructed *Drosophila* optional and mutually exclusive exons as queries. In addition, we examined whether three closely related insects, the German cockroach (*Blattella germanica*), the drywood termite (*Cryptotermes secundus*), and the dampwood termite (*Zootermopsis nevadensis*) showed evidence for splice forms that contain any of these alternate exons. Cockroaches, termites (Blattodea) and grasshoppers (Orthoptera) all belong to the Polyneoptera (Wipfler et al. 2019), and are thus phylogenetically closer to each other than to *Drosophila* (Diptera). Several cDNA sequences corresponding to the *para* locus from *B. germanica* have been isolated and deposited in the NCBI GenBank database (Miyazaki et al. 1996; Dong 1997; Suzuki and Yamato 2018). The *B. germanica*, *C. secundus*, and *Z. nevadensis* genomes and transcriptomes were recently sequenced and assembled (Terrapon et al. 2014; Harrison et al. 2018).

## Results

### Pan-Nav Staining In The Grasshopper Optic Lobe Reveals Axon Fascicles

We used an antibody that recognizes a conserved epitope, pan-Nav, across all vertebrate NaV channel family members to examine whether we could stain for the major NaV channel in the optic lobes of grasshoppers. We observed specific fascicular staining patterns in the optic lobes of each instar and in the adult of *S. americana* (5, 5, 5, 2, 4 and 6 animals for 1st, to 5th instar and adults, respectively, Fig. 1a–f). Staining was relatively diffuse in 1st instars (compare Fig. 1a with Fig. 1b, c), but a regular arrangement of vertical fascicles converging towards the lobula was nonetheless clearly visible at the level of the medulla. In contrast, little specific staining was observed in the lamina. These fascicles likely correspond to axons of descending neurons and their regular arrangement conforms with the modular structure of the medulla, which is subdivided in cartridges processing local information originating from each ommatidium (facet) of the compound eye (Strausfeld 2009). In addition, several larger bundles of axons originating at the level of the lobula of the optic lobe are visible (Fig. 1a–c, >). In the second and

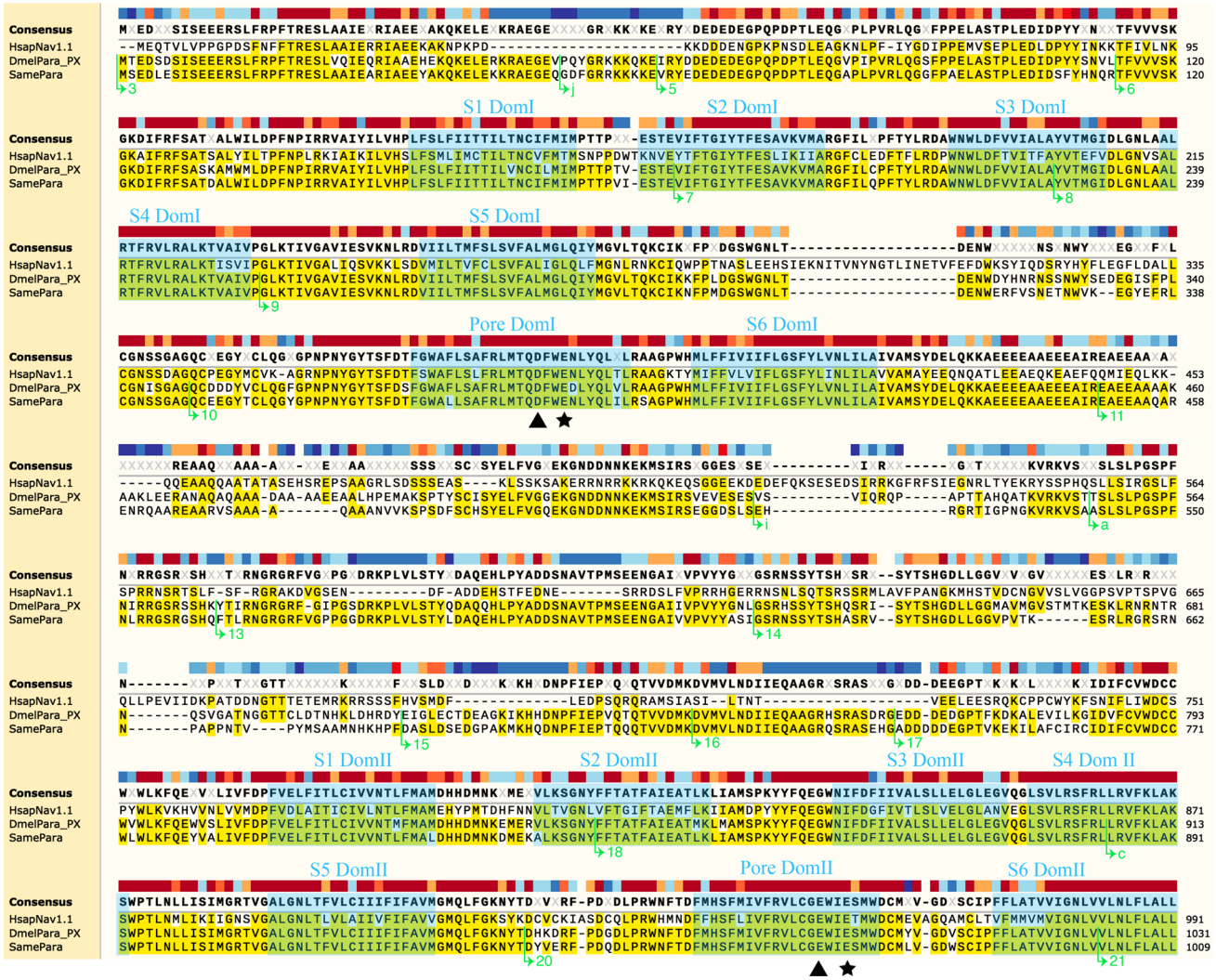


**Fig. 4** NaV channel sequence alignment in *Homo sapiens*, *Drosophila melanogaster* and *Schistocerca americana* from the N-terminus up to the second domain of the protein's 6th transmembrane segment. The top multicolor-coded line identifies the degree of amino acid consensus among the three species sequences. Hot colors (e.g., carmine) signify high consensus and cold colors (e.g., deep blue) low consensus (color bar at bottom of Fig. 5). The second line provides the consensus sequence among the three species. The next line reports the human Para protein sequence (HsapNav1.1), followed by that of *D. melanogaster* (DmelPara_PX) and that of *S. americana* (SamePara). Residues highlighted in yellow are identical across the three species. The sequence portions highlighted in blue correspond to the six transmembrane segments, S1–S6, and the pore region (Pore) for the first two of four domains, DomI–DomIV, of the NaV channel protein (bottom right inset in Fig. 5). Triangle: first two nucleotides constituting the inner pore ring; star: same for outer ring. Green arrows denote the start of the obligatory, optional and mutually exclusive exons in the *para* gene and mRNA. Numbers on right are cumulative amino acid residue counts for each species

third instars the pattern of fascicles was pronounced, and the convergence of these axon bundles was evident from the strong staining at the level of the lobula. In contrast, staining in fourth instars was diffuse and no clear pattern indicative of axons fascicles or axon bundles was reproducibly observed across most of the optic lobe when the brain was fixed for 60 min (Supp. Fig. 2a; 4 animals). Optic lobe staining was also diffuse in 5th instars and adults (4 and 5 animals, respectively; Supp. Fig. 2b, d and e). After trying several variants of the staining protocol, we found that a short, 10 min fixation yielded satisfactory stainings in 4th instars and adults, as well as particularly good ones in 5th instars, generally reproducing the features observed at earlier developmental stages (Fig. 1d–f).

## Pan-Nav staining in the grasshopper central brain clusters along major axonal tracts

Next, we looked at the pattern of pan-Nav staining in the central brain. Figure 2 shows examples of 1st–5th instars

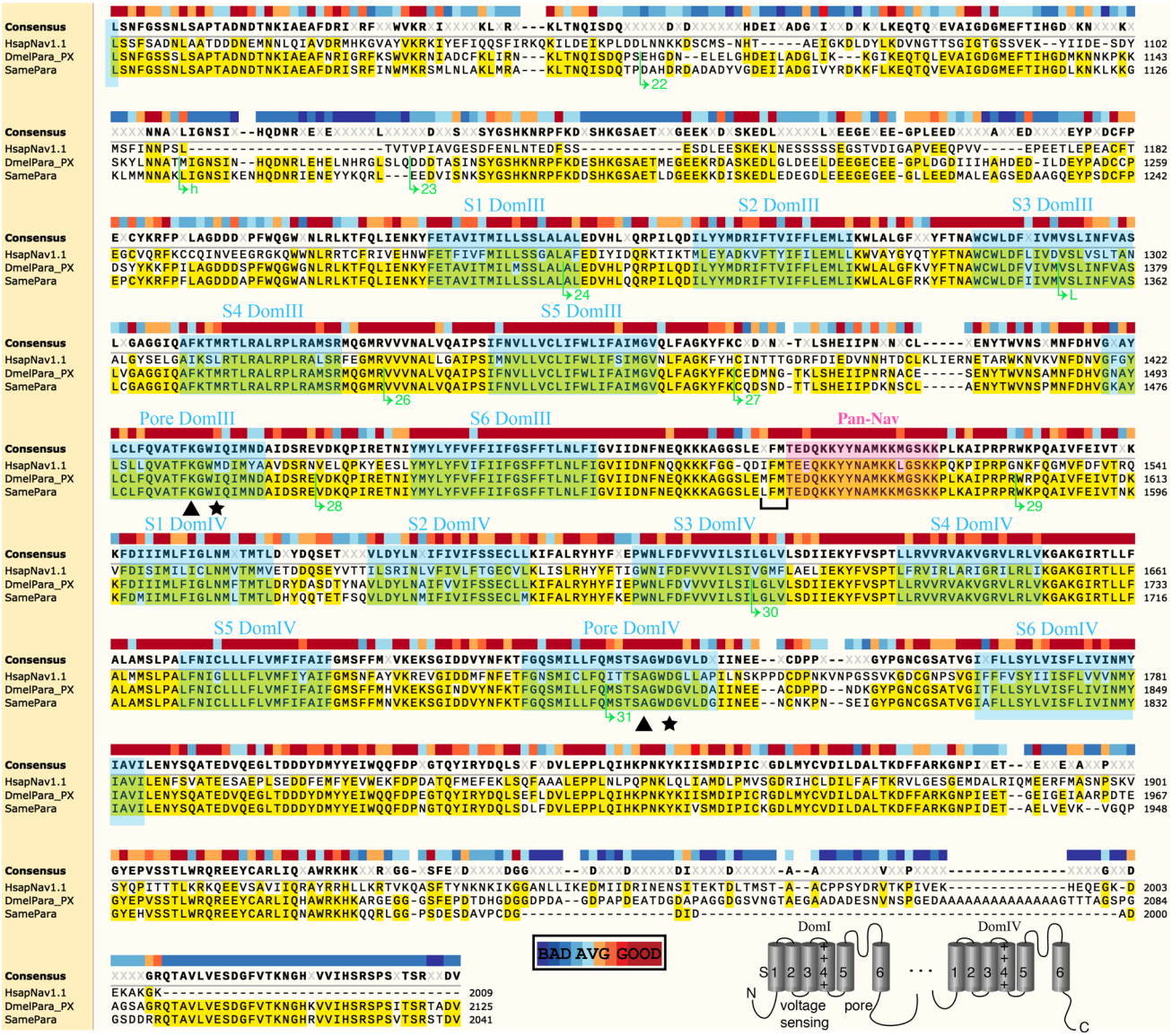


**Fig. 5** NaV channel sequence alignment in *H. sapiens*, *D. melanogaster* and *S. americana* from the second domain of the protein's 6th transmembrane segment up to the C-terminus. The data are presented as in Fig. 4. From top to bottom: the multicolor-coded consensus, the consensus sequence, the human, *Drosophila* and *Schistocerca* sequences. As in Fig. 4, the sequence portions highlighted in blue correspond to S1–S6 and Pore, DomI–DomIV of the protein. The sequence highlighted in pink is the peptide sequence used to generate the pan-Nav antibody. The bottom right inset illustrates schematically the secondary structure of the channel from the N-terminus of the first domain to the C-terminus of the fourth domain. Triangle, star symbols are last two nucleotides of inner and outer pore rings, respectively. Horizontal square bracket indicates inactivation 'lid'. Green arrows and numbers on right as in Fig. 4

and of an adult. Similar results were observed in the same animals used for optic lobe staining. Figure 2a shows the localization of pan-Nav staining in the central brain of a 1st instar. Heavy staining is immediately apparent in the mushroom bodies, a higher center for learning and memory of the olfactory system (Strausfeld 2009). The staining pattern was consistent with the anatomy of the calyx and peduncle of the mushroom body, which contain the axons of an estimated 50,000 Kenyon cells (Jortner et al. 2007). Faint staining was also visible in the central complex. Additional axon bundle tracts were visible running down towards the tritocerebrum. In the 2nd instars (Fig. 2b) the peduncle and calyces of the mushroom bodies were stained heavily, and the fan-shaped body was more clearly outlined than in the 1st instar brain. Supp. Movie 1, assembled from an image stack acquired across the central brain, sharply illustrates the three-dimensional structure of additional bundle tracts in the central brain. A similar pattern of staining was observed in the 3rd instars (Fig. 2c) but here we observed a clear outline of the antennal lobes based on a series of stained

fascicles inside and around them. In the 4th instars staining could still clearly be seen in the mushroom bodies and the antennal lobes, although axon tracts were not as well resolved (Fig. 2d). Additionally, the olfactory antennal nerves were strongly stained, consistent with the presence of a large number of olfactory receptor neuron axons. This resolved pattern of staining contrasted with the diffuse pattern observed in the optic lobe of the 4$^{th}$ instars when fixation lasted 60 min (see above). In the 5th instars, only diffuse staining was observed in the central brain when fixing for the same duration (Supp. Fig. 2c; four animals). Similar results were observed in adults (five animals; not shown). The lack of specific staining in later instars and adults might have been caused by decreased penetration of the antibody in thicker brain tissue (i.e., decreased diffusion into the fixed tissue, Thurber et al. 2008). However, this appears unlikely given the differential staining of the central brain and optic lobes in the 4th instars. To further rule out this possibility, we carried out simultaneous pan-Nav and 5-HT (serotonin) immunofluorescence staining in adult grasshoppers (2 animals). While the optic lobes showed diffuse staining to pan-Nav (see above), we could resolve staining to 5-HT (Supp. Fig. 2d, e). In contrast, a short fixation time of 10 min largely reproduced in 5th instars and in adults the results observed with longer fixation times in 1st–4th instars (Fig. 2e, f; four animals).

## Short fixation time reveals matching Para localization pattern in vinegar flies

As in adult and 5th instar grasshoppers, staining either *Drosophila* adults (Supp. Figure 3a; 6 animals) or larvae (Supp. Fig. 3d; five animals) with pan-Nav following 60 min fixation showed predominantly diffuse patterns, although part of the mushroom body calyces and motor neuron axons could be resolved in L3 larvae. Based on the observations made in grasshoppers, we tested successively shorter fixation times. With 15 min fixation, a slight improvement was observed in adults (Supp. Fig. 3b; three animals). The same held true for L3 larvae (Supp. Fig. 3e; three animals). In contrast, we observed in both cases well resolved neurite projections when staining for 5-HT using the same fixation times (Supp. Fig. 3c, f; three and three animals, resp.). An even shorter, 5 min fixation resulted in a large number of well resolved anatomical features in adults (Fig. 3a; 11 animals, Supp. Movie 2). Imaging the optic lobes at higher magnification, revealed the presence of fascicles similar to those observed in grasshoppers at the level of the medulla but none in the lamina (Fig. 3b; c.f. Fig. 1). Individual images from acquired stacks showed different types of transmedullary neuron stained in the optic lobes (Supp. Movie 3). To further resolve the identity of the stained neurons, we stained brains expressing GFP in medullary T4 and lobula T5 neurons using *GMR42F06-GAL4 > UAS-GFP* flies (Jenett et al. 2012; Maisak et al. 2013; Thurmond et al. 2019). Although we saw some overlap between the GFP signal and pan-Nav, we also observed Para localization outside of the T4/T5 neurons (Supp. Fig. 4a, b, Supp. Movie 2, 3). In the central brain, the mushroom body peduncles were apparent as well as a large number of thick fascicles and commissures (Fig. 3a, c). In the maximum intensity projection of the brain some fascicles belonging to the central complex could be resolved, such as the fan-shaped body (Fig. 3c). In a movie of stacked projections these fascicles outlining the entire central complex were very well resolved as well as large fascicular bundles and commissures throughout the entire central brain (Supp. Movie 4). Fascicles were also clearly visible in the lateral protocerebrum and the sub esophageal zone. The overall pattern of these bundles in the central brain was reminiscent of the intricate pattern documented in *Musca* and *Drosophila* by classical anatomical methods (Strausfeld 2009; Ito et al. 2014). We also stained the ventral nerve cord of the adult and could visualize fascicles throughout although they are less pronounced than in the brain (Fig. 3d, Supp. Movie 5). In L3 larvae, fascicular bundles became visible in the ventral nerve cord and the central brain when fixation times were reduced to 5 min although they were less well resolved than in the adult brain (Supp. Fig. 3g). Shortening the fixation time further to 2 min did not improve the results in larvae (Supp. Fig. 3h, five animals). In all of the larval and adult *Drosophila* brain preparations, we observed staining in cell bodies localized to the cortex surrounding each neuropil. We did not observe such somatic signals in the grasshopper brains. The fascicular stainings described above closely match those recently reported in an endogenously GFP-tagged Para reporter strain (Ravenscroft and Bellen 2019, personal communication, 2019 Neurobiology of Drosophila Cold Spring Harbor Meeting; Venken et al. 2011).

## High level of homology between *Drosophila* and *Schistocerca* sequences

Given the robust staining observed in grasshoppers and vinegar flies, we investigated the molecular composition of NaV channels in grasshoppers. We used the Para isoform sequences of *Drosophila* to identify potential orthologs in the head and thorax transcriptome of *S. americana*. This allowed us to assemble a complete *S. americana* Para sequence depicted in Figs. 4 and 5. The sequence was aligned with that of *Drosophila melanogaster*'s closest isoform, Para PX, and with that of Nav1.1, one of *Homo sapiens*' NaV channel orthologs expressed in central neurons. We used the known location of the transmembrane segments S1–S6 for each of the four domains of the channel (DomI–DomIV) in *Drosophila* and *Homo* to identify

their location in *Schistocerca*. Figure 4 shows that segments S1–S6 of the first two domains are highly conserved between *S. americana* and *D. melanogaster*, with only 6 out of 233 amino acids differing (2.6%). Similarly, segments S1–S6 of the last two domains differed from those of *D. melanogaster* by only 9 out of 230 amino acids (3.9%; Fig. 5). In addition, the $Na^+$ selectivity filter amino acid sequence 'DEKA' which forms an inner ring distributed across the four pore domains was conserved across all three species (Heinemann et al. 1992; Catterall 2000; Figs. 4, 5 arrowheads). In contrast, the methionine of the vertebrate outer ring sequence 'EEMD' involved in channel permeability (Chiamvimonvat et al. 1996) and sensitivity to TTX (Terlau et al. 1991) was substituted by an isoleucine in *S. americana*, as is the case in *D. melanogaster* (Figs. 4, 5, star). In vertebrates, a short hydrophobic amino acid sequence 'IFM', located in the intracellular loop between the last two transmembrane domains, plays a critical role in fast inactivation of the channel through interactions with domain IV (Fig. 5, horizontal square bracket; West et al. 1992; Catterall 2000; Capes et al. 2013; Pan et al. 2018; Clairfeuille et al. 2019). The equivalent insect amino acid sequence is MFM in *Drosophila* and several other insects (Dong et al. 2014). In contrast, the first amino acid is substituted by leucine in *Schistocerca*, which is closely related to the above-mentioned isoleucine (vertebrates) and methionine (insects). Immediately downstream of this tripeptide lies the peptide sequence used to generate the pan-Nav antibody, which was identical in *S. americana* and *D. melanogaster* and differed only by two of eighteen amino acids from that in *H. sapiens* (Fig. 5). Outside these transmembrane and pore regions, the sequence was less conserved, with the highest variability observed at the amino and carboxyl termini, the segment between domains I and II, and the segment between domains II and III, as is also the case in vertebrates (Soderlund 2005). On average, there was 75% identity between *D. melanogaster* and *S. americana*, which is on the lower end of that observed in other insects that have been compared to *D. melanogaster* (e.g., *Anopheles gambiae* 82%, Davies et al. 2007; *Periplaneta americana* 81%, Moignot et al. 2009; *Bombyx mori* 74%, Shao et al. 2009). Similarly, homology between *S. americana* Para and *H. sapiens* Nav1.1 was on average 43.2%, while that of *D. melanogaster* was 41.6%.

As we had transcriptomes for both head and thorax tissue, we compared their *para* expression levels. The expression of the *para* gene was 5.2 times higher in head than in thorax tissue in last instar nymphs (TPM values of 0.344 and 0.067, respectively). These values show that *para* is a lowly expressed gene: in comparison, the actin gene has TPM values of 104.83 and 181.45, respectively, for head and thorax tissue. This is likely due to specific expression of *para* in neural tissue, while our transcriptomes originated from whole head and whole thorax tissue.

### *Para* splice variants in *Schistocerca*, *Blatella*, *Cryptotermes*, and *Zootermopsis*

In *Drosophila*, a large number of *para* splice variants have been reported (Loughney et al. 1989; Lin et al. 2009; Dong et al. 2014; Thurmond et al. 2019). To characterize those in grasshoppers, we started by compiling a list of the complete amino acid sequences of obligatory, optional and mutually exclusive exons of the *Drosophila para* locus using the Para isoform sequences available in FlyBase (Thurmond et al. 2019). Figure 6a shows the structure of the *Drosophila para* locus. Obligatory coding exons are numbered from 3 to 31 (the first two exons are non-coding). In addition, the locus contains 7 optional exons denoted by the letters j, i, a, b, e, f and h (Lin et al. 2009; Dong et al. 2014) as well as two pairs of mutually exclusive exons denoted by the letters c, d (pair 1) and k, L (pair 2), respectively. Table 1 lists the amino acid sequence of all these exons and their corresponding base pairs in the *para* locus. The *Drosophila* Para isoform PX depicted in Figs. 4 and 5 contains all numbered obligatory exons and alternative exons j, i, a, c, h and L. In these two figures, a right-angled green arrow indicates the start location of each exon by its associated label. For example, immediately after exon 3 at the start of the sequence, the second coding exon of Para PX is exon j, which starts with the amino acid phenylalanine (Fig. 4 top line and Table 1). The mapping between the 60 Para isoforms documented in FlyBase and the alternatively spliced exons of *para* is given in Table 2. FlyBase shows isoforms that vary in exon 7, encoding part of transmembrane segments 2 and 3 in domain I of the channel (Fig. 4, second line). It also contains five isoforms of the channel truncated after exon 6, exon d or exon 18 (PAR, PAU, PAV, PBC and PBE, Table 2). Figure 6b maps Para domain transmembrane segments and the pan-Nav sequence onto specific exons of the *Drosophila para* locus.

By combining this information with the most common reads of our RNA-seq data, we assembled a primary Para isoform in *Schistocerca* that contains some of the optional and mutually exclusive *Drosophila* exons (Fig. 6c). Specifically, it contains the 4 optional exons, j, i, a and h and exons c and L of the mutually exclusive pairs (c, d) and (k, L) in *Drosophila*. In *Schistocerca*, our data indicates that exon L is mutually exclusive with exon k. However, we found no evidence for the existence of exon d (see below) and it thus seems that exon c is obligatory in *Schistocerca* and not mutually exclusive with exon d, in contrast to the situation in *Drosophila*. We also compared these exon sequences with those of three additional species of Polyneoptera, *Blattella germanica*, *Cryptotermes secundus*, and *Zootermopsis nevadensis*, which are phylogenetically closer to each other and to *Schistocerca* than to *Drosophila* (see "Material and methods"). In general, the sequences encoded by the

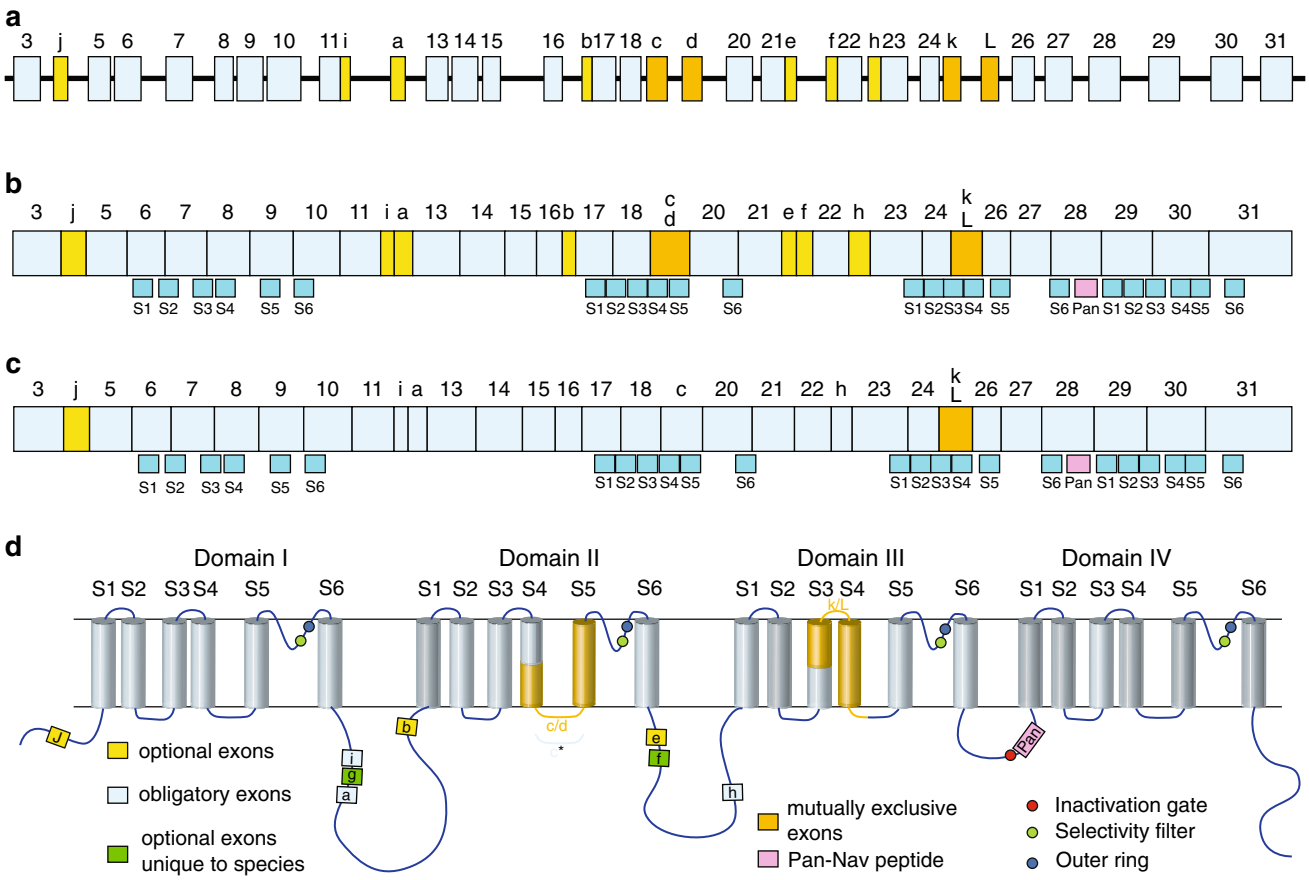


**Fig. 6** **a** Diagram of the intron–exon structure of the *para* gene in *Drosophila* (boxes represent coding exons). Optional exons are shown in yellow and mutually exclusive exons are shown in orange. Transcript corresponding to a splice form containing all the optional exons in *Drosophila* (**b**) compared to the *para* splice form in *Schistocerca* (**c**) assembled from our RNA-seq data. The localization of the transmembrane domains and pan-Nav sequence are depicted below the exons in blue boxes and a pink box, respectively. **d** Secondary Para protein structure of the different domains corresponding to the transcripts above is shown in cartoon form, depicting in color the optional and mutually exclusive exons as yellow boxes and orange barrels, respectively. The blue boxes represent optional exons in *Drosophila* that are obligatory in Polyneoptera (exons i, a and h). The green boxes represent optional exons that are species specific (exon g in Polyneoptera and exon f in *Drosophila*). Of the mutually exclusive exons c/d, only exon c is present in Polyneoptera and no isoforms with exon d were detected (denoted by an asterisk in the diagram). The inactivation gate and adjacent pan-Nav sequences as well as the selectivity filter and outer ring are also shown on the cartoon (see labels). For detailed sequence information see also Table 1

different exons differ in their amino acid composition from those found in *Drosophila*, as summarized in Table 3 and in alignments between the different species (Supp. Figure 5).

Furthermore, analysis of our sequence reads identified transcripts missing exon j in the *Schistocerca* transcriptome from thorax tissue, while all transcripts from head tissue contain exon j. In *Blattella* one of the 5 known isoforms contains exon j, in the dampwood termite approximately half of its 22 known isoforms do, while in the drywood termite none of its 14 known isoforms have this exon. Together these results suggest that exon j is also optional in Polyneoptera. The Para exon j encoded sequence is highly conserved across the Polyneopteran species but only about half of the residues are identical to those of the vinegar fly (Table 3 and Supp. Fig. 4). While exons i and a are optional in *Drosophila* (Table 2), we found no transcript reads without these exons in grasshoppers or the other Polyneopteran species, suggesting that they are not optional in these insects. However, in a subset of the cockroach and termite isoforms, exons i and a are interrupted by a novel optional exon not present in *Drosophila*, that we have termed exon g (Table 3, Supp. Fig. 5). This exon is weakly homologous to an optional exon in the same location in *B. mori* Para (Shao et al. 2009). Although we found reads in *S. americana* that correspond to exon g in frame with the exon i sequence, they were either truncated downstream or in frame spliced midway to the next exon following exon a. For optional exon b, we found no corresponding reads in grasshopper, but about half the cockroach and termite isoforms contain exon b, with only one residue difference compared to the *Drosophila* sequence (Table 3, Supp. Fig. 4). We also found reads corresponding to optional exon e in our grasshopper data. While we found

**Table 1** *Drosophila melanogaster* Para coding exons

| | Exon sequence | Start | End | Size | Intron size |
|---|---|---|---|---|---|
| 3 | MTEDSDSISEEERSLFRPFTRESLVQIEQRIAAEHEKQKELERKRAEGEV | 17,349 | 17,498 | 191 | 2795 |
| j | PQYGRKKKQKE | 20,284 | 20,316 | 33 | 4620 |
| 5 | IRYDDEDEDEGPQPDPTLEQGVPIPVRLQGSFPPELASTPLEDIDPYYSNVL | 24,937 | 25,092 | 156 | 109 |
| 6 | TFVVVSKGKDIFRFSASKAMWMLDPFNPIRRVAIYILVHPLFSLFIITTILVNCILMIMPTTPT VESTE | 25,201 | 25,406 | 206 | 4011 |
| 7 | VIFTGIYTFESAVKVMARGFILCPFTYLRDAWNWLDFVVIALA | 29,417 | 29,545 | 129 | 3135 |
| 8 | YVTMGIDLGNLAALRTFRVLRALKTVAIVP | 32,682 | 32,773 | 92 | 100 |
| 9 | GLKTIVGAVIESVKNLRDVIILTMFSLSVFALMGLQIYMGVLTQKCIKKFPLDGSWGNLTDEN WDYHNR NSSNWYSEDEGISFPLCGNISGAG | 32,874 | 33,150 | 277 | 155 |
| 10 | QCDDDYVCLQGFGPNPNYGYTSFDSFGWAFLSAFRLMTQDFWEDLYQLVLRAAGPWHM LFFIVIIFL GSFYLVNLILAIVAMSYDELQKKAEEEEAAEEEAIR | 33,305 | 33,614 | 310 | 1209 |
| 11 | EAEEAAAAKAAKLEERANAQAQAAADAAAAEEAALHPEMAKSPTYSCISYELFVGGEK GNDDNNKEK MSIRSVEVESES | 34,824 | 35,059 | 237 | 0 |
| i | VSVIQRQPAPTTAHQATKVRKVST | 35,060 | 35,131 | 71 | 3421 |
| a | TSLSLPGSPFNIRRGSRSSHK | 38,552 | 38,614 | 63 | 1610 |
| 13 | YTIRNGRGRFGIPGSDRKPLVLSTYQDAQQHLPYADDSNAVTPMSEENGAIIVPVYYGNL | 40,225 | 40,405 | 181 | 58 |
| 14 | GSRHSSYTSHQSRISYTSHGDLLGGMAVMGVSTMTKESKLRNRNTRNQSVGATNG- GTTCLDTNHKL DHRDY | 40,465 | 40,676 | 212 | 74 |
| 15 | EIGLECTDEAGKIKHHDNPFIEPVQTQTVVDMK | 40,752 | 40,851 | 100 | 5754 |
| 16 | DVMVLNDIIEQAAGRHSRASDRG | 46,606 | 46,674 | 69 | 2569 |
| b | VSVYYFPT | 49,244 | 49,267 | 24 | 0 |
| 17 | EDDDEDGPTFKDKALEVILKGIDVFCVWDCCWVVWLKFQEWVSLIVFDPFVELFITLCIVVNT MFMAMD HHDMNKEMERVLKSGNY | 49,268 | 49,521 | 254 | 83 |
| 18 | FFTATFAIEATMKLMAMSPKYYFQEGWNIFDFIIVALSLLELGLEGVQGLSVLRSFRL | 49,605 | 49,778 | 174 | 194 |
| **c** | LRVFKLAKSWPTLNLLISIMGRT**V**GALGNLTFVLCIIIFIFAVMGMQLFGKNY**T** | 49,972 | 50,134 | 163 | 941 |
| **d** | LRVFKLAKSWPTLNLLISIMGRTMGALGNLTFVLCIIIFIFAVMGMQLFGKNYH | 51,076 | 51,238 | 163 | 976 |
| 20 | DHKDRFPDGDLPRWNFTDFMHSFMIVFRVLCGEWIESMWDCMYVGDVSCIPFFLATVVI GNLV | 52,216 | 52,403 | 188 | 132 |
| 21 | VLNLFLALLLSNFGSSSLSAPTADNDTNKIAEAFNRIGRFKSWVKRNIADCFKLIRNKLTNQIS DQPS | 52,537 | 52,741 | 205 | 0 |
| e | GERTNQISWIWSE | 52,742 | 52,780 | 39 | 2452 |
| f | GKGVCRCISA | 55,232 | 55,261 | 30 | 0 |
| 22 | EHGDNELELGHDEILADGLIKKGIKEQTQLEVAIGDGMEFTIHGDMKNNKPKKSKYLNNAT | 55,262 | 55,443 | 182 | 569 |
| h | MIGNSINHQDNRLEHELNHRGLSLQ | 56,013 | 56,087 | 74 | 0 |
| 23 | DDDTASINSYGSHKNRPFKDESHKGSAETMEGEEKRDASKEDLGLDEELDEEGECEEGPLDG DIIIHA HDEDILDEYPADCCPDSYYKKFPILAGDDDSPFWQGWGNLRLKTFQLIENKYFE TAVITMILMSSLAL | 56,088 | 56,495 | 408 | 1127 |
| 24 | ALEDVHLPQRPILQDILYYMDRIFTVIFFLEMLIKWLALGFKVYFTNAWCWLDFVIVM | 57,622 | 57,795 | 174 | 523 |
| **k** | **L**SLIN**LA**A**VWS**GA**DDVP**AF**RS**MRTLRALRPLRA**V**SR**WE**GMK | 58,319 | 58,441 | 123 | 3107 |
| **L** | VSLINFVASLVGAGGIQAFKTMRTLRALRPLRAMSRMQGMR | 61,550 | 61,672 | 123 | 1698 |
| 26 | VVVNALVQAIPSIFNVLLVCLIFWLIFAIMGVQLFAGKYFK | 63,371 | 63,493 | 123 | 986 |
| 27 | CEDMNGTKLSHEIIPNRNACESENYTWVNSAMNFDHVGNAYLCLFQVATFKGWIQIMN DAIDSRE | 64,480 | 64,674 | 195 | 619 |
| 28 | VDKQPIRETNIYMYLYFVFFIIFGSFFTLNLFIGVIIDNFNEQKKKAGGSLEMFMTEDQK KYYNAMKKMGSKKPLKAIPRPR | 65,294 | 65,539 | 246 | 2089 |
| 29 | WRPQAIVFEIVTDKKFDIIIMLFIGLNMFTMTLDRYDASDTYNAVLDYLNAIFVVIFSSECLLKI FALRYHYFIEPWNLFDVVVVILSIL | 67,637 | 67,907 | 271 | 4414 |
| 30 | GLVLSDIIEKYFVSPTLLRVVRVAKVGRVLRLVKGAKGIRTLLFALAMSLPALFNICLLLFLVM FIFAIFGMSFFMHVKEKSGINDVYNFKTFGQSMILLFQ | 72,322 | 72,626 | 305 | 1702 |

**Table 1** (continued)

| | Exon sequence | Start | End | Size | Intron size |
|---|---|---|---|---|---|
| 31 | MSTSAGWDGVLDAIINEEACDPPDNDKGYPGNCGSATVGITFLLSYLVISFLIVINMYIA VILENYSQATE DVQEGLTDDDYDMYYEIWQQFDPEGTQYIRYDQLSEFLDVLEPPL QIHKPNKYKIISMDIPICRGDLMY CVDILDALTKDFFARKGNPIEETGEIGEIAARPDT EGYEPVSSTLWRQREEYCARLIQHAWRKHKARG EGGGSFEPDTDHGDGGDPDAGDPAP DEATDGDAPAGGDGSVNGTAEGAADADESNVNSPGEDAAAAAAAAAAAAAAGTTTAGSP GAGSAGRQTAVLVESDGFVTKNGHKVVIHSRSPSITSRTADV | 74,329 | 75,333 | 1005 | |

The first coding exon in the *para* locus is exon 3. All exons are numbered up from there except for the optional and mutually exclusive exons that are designated by letters. Adjacent mutually exclusive exons are in bold. Exons i and e use differential splice donors, while exons b, f and h use differential splice acceptors and their sequences are part of a numbered exon. The other optional or mutually exclusive exons are fully independent exons and replace a numbered exon. Bold font residues in exons c and k show the differences with their mutually exclusive counterpart (d and L, respectively). Start and end refer to nucleotide number in the *D. mel. para* locus SnapGene file (Supplementary Data File). Size is the nucleotide length of the exon. Intron Size is the length of the intron immediately following the exon (see Fig. 6a)

**Table 2** Alternatively-spliced exons in *Drosophila melanogaster* Para isoforms

| Isoform | | Isoform | | Isoform | |
|---|---|---|---|---|---|
| PA | j i a b d e f L | PAT | No-7 i b d e f L | PG | j i b d L |
| PAA | j a d L | PAU | No-7 i b d truncated | PH | i a b d L |
| PAB | j a c f L | PAV | No-7 i b d truncated | PI | j i d L |
| PAC | j a b d L | PAW | b d f L | PJ | j i a c L |
| PAD | i b d f k | PAX | i a d f L | PK | j a c L |
| PAE | j i a b d k | PAY | i a d f h k | PL | j i b c L |
| PAF | i a b d e L | PAZ | i b d f h k | PM | j i a d L |
| PAG | i b d e L | PB | j i a b d e f k | PN | j i b d e L |
| PAH | i a b d f L | PBA | i a b c f h L | PO | j i d e L |
| PAI | i b d f L | PBB | i a b d f | PP | j i a b d e L |
| PAJ | i a b d f h L | PBC | truncated after 18 | PQ | j a d L |
| PAK | i a b d L | PBD | i a b d | PR | j i c L |
| PAL | i b d f h L | PBE | i a truncated after 18 | PS | j i a b c e L |
| PAM | a b d f L | PBF | j i a b d e f L | PT | j i a d f L |
| PAN | j i a b d f h L | PBG | j i a b d e f L | PU | j i a b d f L |
| PAO | j i a d e L | PBH | i a b d | PV | j i b d f L |
| PAP | j i b d f k | PC | j i a b c e f L | PW | j i d e f L |
| PAQ | j i d f L | PD | i a c h k | PX | j i a c h L |
| PAR | 3 5 6 truncated | PE | j i a b d L | PY | j i a c e h L |
| PAS | No-7 i a b d e L | PF | j i a b c L | PZ | j a c e L |

Lin et al. (2009) describe isoforms lacking exon 8 although none are found in FlyBase

no cockroach isoforms with this sequence, about half the termite isoforms contain this optional exon. Its sequence is identical across grasshoppers and termites, but very degenerate compared to the *Drosophila* sequence (Table 3, Supp. Fig. 4). None of the Polyneoptera shows evidence for optional exon f, but two of the annotated *Cryptotermes* isoforms lack the first 12 residues encoded by exon 22, and we tentatively termed this alternative splice form as exon m (Table 3). The final optional exon in *Drosophila* is exon h. Like exons i and a, it is present in all isoforms of grasshoppers, cockroach and termites. Even within Polyneoptera its sequence only shows about 50% identity (Table 3, Supp. Fig. 4). The first set of mutually exclusive exons in *Drosophila*, exons c and d, encode the second half of transmembrane segment S4 through S5 of domain II and the first half of the loop that makes up the pore domain of the channel (Fig. 4, last two rows; Fig. 6c). In *Drosophila*, these exons only differ by 2 of 54 residues (Table 3, red letters V and T). In Polyneopteran species, we found evidence for a single exon c that differs from that of *Drosophila* only in the last residue (Table 3, Supp. Fig. 4). The second set of mutually exclusive exons in *Drosophila*, exons k and L, encode part of transmembrane segment S3 through the complete S4 of domain III and part of the subsequent intracellular loop of

**Table 3** Alternatively-spliced coding exons in *Drosophila*, *Schistocerca*, *Blatella*, and *Cryptotermes* Para

| | *D. melanogaster* | *S. americana* | *B. germanica* | *C. secundus* |
|---|---|---|---|---|
| Exon j | PQYGRKKKQKE | QGDFGRRKKKE | GDFGRRKKKKE | |
| Exon i* | VSVIQRQPAPTTAHQAT KVRKVST | LSEHRGRTIGPNGKVRKVSA | ISEHKGRVGANGTAIRKVSA | ISEHRGRIAGANGSM VRKVSA |
| Exon g | | VPCQYRDYTATKRQLTF SYQENLMK | VPQFRDTKTATKSQFT FAYQENLVK | VPHCQYRDSNTATKSQFT FTYPESLVK |
| Exon a* | TSLSLPGSPFNIRRGSRSSHK | ASLSLPGSPFNLRRGSRG SHQ | ASLSLPGSPFNHRRGSQG SHH | ASLSLPGSPFNLRRGSRG SHQ |
| Exon b | VSVYYFPT | | VSIYYFPT | VSIYYFPT |
| **Exon c*** | LRVFKLAKSWPTLNL LISIMGRT**V**GALGNLTF VLCIIIFIFAVMGMQLF GKNY**T** | LRVFKLAKSWPTLNLLI SIMGRTVGALGNLTFV LCIIIFIFAVMGMQLFG KNYT | LRVFKLAKSWPTLNL LISIMGRTVGALGNLT FVLCIIIFIFAV MGMQLF GKNYY | LRVFKLAKSWPTLNLLI SIMGRTVGALGNLTFV LCIIIFIF AVMGMQLFG KNYG |
| **Exon d** | LRVFKLAKSWPTLNL LISIMGRTMGALGNLTF VLCIIIFIFAVMGMQLF GKNYH | | | |
| Exon e | GERTNQISWIWSE | GEGPSSSWKE | | GEGPSSSWKE |
| Exon m | | | | DAHEHDTDLDL |
| Exon f | GKGVCRCISA | | | |
| Exon h* | MIGNSINHQDNRLEHEL NHRGLSLQ | LIGNSIKENHQDN RIENEYYKQRL | VIGNSLNHKDNRIESGDYL HNRQ | VIGNSFQGNHKDNRIENEY LHNRQ |
| **Exon k** | **L**SLIN**LA**A**V**F**WS**GA**DDVP**A F**RS**MRTLRALRPLRA**V**SR **WE**GMK | LSLINLAAIWAGAADIPA FRSMRTLRALRPLRAVSR WEGMR | | LSLINLTAVWTGAADIPA FRSMRTLRALRPLRAVSR WEGMR |
| **Exon L** | VSLINFVASLVGAGGIQAFK TMRTLRALRPLRAM SRMQGMR | VSLINFVASLCGAGGIQAFK TMRTLRALRPLRAM SRMQGMR | VSLINFVASLVGAGGIQAFK TMRTLRALRPLRAM SRMQGMR | VSLINFVASLAGAG GIQAFKTMRTLRALRPL RAMSRMQGMR |

Adjacent exons in bold font are mutually exclusive exons. Other exons are optional. Bold font residues in *Drosophila* Para exons c and k show the differences with their mutually exclusive counterpart (d and L, respectively). Empty cells indicate there is no evidence to support the existence of that exon in the species corresponding to that column. Exons denoted with an asterisk (*) are obligatory in Polyneopterans

the channel (Fig. 5, third row; Fig. 6b). In contrast to the mutually exclusive exons c and d, exons k and L differ from each other more substantially in *Drosophila* (1/3 of the 41 residues are different). We found reads in grasshopper corresponding to both alternative exons. While the GenBank *Blattella* isoforms all use exon L, the isoforms from both termite species either contain exon k or L. The exon L sequences of the different species only differ in 1 of the 41 residues, while the exon k sequences have 6 residue differences (Table 3, Supp. Fig. 4). We found 1 transcript in our grasshopper reads that contains both exon k and L. One deposited *Z. nevadensis* isoform shares this k plus L configuration. Finally, in *Drosophila* several isoforms are annotated as missing exon 7 (Table 2). We found no isoforms missing this exon in *Schistocerca* but two of the *Cryptotermes* isoforms lack exon 7. In summary, the splice structure of Polyneoptera is relatively consistent across species but differs substantially from that of *Drosophila*.

## Discussion

Voltage-gated sodium (NaV) channels play a critical role for spike propagation in the central nervous system. Up to now, no information was available on their spatial localization in the brain of insects. In vertebrates, sodium channel antibodies stain bundles of unmyelinated axonal fibers in the central and peripheral nervous system (Gong et al. 1999; Henry et al. 2012; Su et al. 2013). Our immunostainings reveal the existence of similar well-resolved fiber tracts across the brain and the optic lobes of *Schistocerca* and *Drosophila*. In the central brain of grasshoppers, the most striking localization of NaV channels was in the peduncle of the mushroom body (MB). The MB peduncles contain the axons of Kenyon cells projecting to the MB lobes, where they contact MB output neurons (MacLeod et al. 1998) expected to drive olfactory learning (Simões et al. 2011; Saha et al. 2013). Kenyon cells fire sparsely in response to olfactory input and are thought to use a temporal code to discriminate olfactory stimuli (Perez-Orive et al. 2002). The high density of NaV channels in their

axons evidenced in our stains would help maintain the reliability of such a temporal code. In *Drosophila*, the MB peduncles were not as clearly resolved in single projection images but could be followed in movies assembled from stacks of images acquired through the central brain. In the optic lobes of *Schistocerca* and *Drosophila*, NaV channels were distributed along fascicles in the medulla that we interpret as axon bundles of transmedullary neurons projecting to the lobula complex. In grasshoppers, axon bundles originating in the lobula complex were also stained, suggesting that part of the information exiting the lobula complex rapidly propagates across sizable distances, e.g., toward thoracic motor centers. In contrast to *Schistocerca*, we detected pan-Nav staining in the somata of *Drosophila* neurons. This was unexpected as the somata of insect neurons are generally not excitable. While the cell body staining may represent an artefact, somatic staining has been reported with other ion channel antibodies (Hu et al. 2015; Xiao et al. 2017) and may result from immature protein precursors (Redondo et al. 2013).

In both *Schistocerca* and *Drosophila*, pan-Nav immunostaining offered sufficient contrast to resolve neuropils such as the antennal lobes, the central complex and its fan-shaped body. It is possible that the lighter stains observed in these structures and across the brain reflect in part a lower density of sodium channels in neuronal dendrites. However, in the hippocampus the density of sodium channels in dendrites was estimated to be 35–80 times lower than in axons and could only be reliably resolved by electron microscopical techniques (Lorincz and Nusser 2010). In CA1 pyramidal cells, these dendritic sodium channels contribute to dendritic action potential backpropagation in the context of synaptic plasticity. In the grasshopper LGMD neuron, action potentials backpropagating from the spike initiation zone (SIZ) along the main neurite and within the dendrites have been documented (Dewell and Gabbiani 2019). Biophysical modeling suggests that NaV channels located along the main LGMD neurite and decreasing in density as distance from the SIZ increases are required to explain such action potential backpropagation (Dewell and Gabbiani 2018, 2019). More generally, invertebrate neurons including those of insects are known to possess one and sometimes multiple SIZs as evidenced by a variety of techniques (e.g., O'Shea 1975; Peron and Gabbiani 2009; Trunova et al. 2011; Kuehn and Duch 2013; Günay et al. 2015). Backpropagating action potentials are also expected to play a role in spike-timing dependent plasticity in insects (Feldman 2012).

Several earlier investigations have indicated the presence of sodium channels in the insect brain. In *S. americana* antibodies against the same peptide sequence targeted in this study detected NaV channels by immunoprecipitation using a radiolabeled probe (Gordon et al. 1988). In *Drosophila*, in situ hybridization has shown the presence of para mRNA in parts of the central brain (Hong and Ganetzky 1994) and more recently a polyclonal antibody was able to detect coarse changes in Para protein expression levels (Xiao et al. 2017). However, none of these studies had sufficient spatial resolution to identify the fine structure of Para distribution in the brain, particularly the bundles of central brain axons and the stereotypically repeated optic lobe fascicles evidenced here. Thus, our study is the first to identify NaV channel localization in grasshoppers and vinegar flies. In vinegar flies our results are in close agreement with and complement those obtained by genetic techniques (Ravenscroft and Bellen 2019, personal communication).

In future work we see at least two ways in which our immunostaining results could be improved. First, it would be beneficial to combine immunostaining for NaV channels with simultaneous neuropil staining. This would allow unambiguous identification of the axon bundles revealed here by matching their localization relative to known neuropils with axon tract information available from anatomical atlases of the *Drosophila* and *Schistocerca* brains (Kurylas et al. 2008; El Jundi et al. 2010; Ito et al. 2014). We did not carry out such dual stains, because the pan-Nav antibody requires a secondary anti-mouse antibody as do most neuropil markers. However, this is a technical issue that can be resolved. Second, the short fixation times required to visualize sodium channels indicate that formaldehyde fixation masks the antigens targeted by the pan-Nav antibody, a well-known issue (Dapson 2007; Lorincz and Nusser 2008). Various possibilities exist to correct this problem, including antibody retrieval techniques (Lorincz and Nusser 2008; Ramos-Vara and Miller 2014), the use of low pH fixation conditions (Lorincz and Nusser 2010), and zinc formalin fixation (Ott 2008; Dapson 2010). Identifying the best method is likely to be time consuming but might open the possibility of mapping the subcellular localization of NaV channels in single cells such as the LGMD, at least in axons. In *Drosophila*, clonal analysis with driver lines that show clear expression in neuropil regions stained with pan-Nav may also resolve subcellular regions of NaV channel distribution.

Identifying Para in *S. americana* required us to update and synthesize information about *Drosophila* Para scattered across the literature. The *S. americana* Para protein finally identified from transcriptome data exhibited a high degree of homology with that of *D. melanogaster* and the human Nav1.1 sequence over the transmembrane domains critical to its function. Outside those domains, divergence from *D. melanogaster*'s Para sequence was higher, in agreement with the evolutionary distance of these species, thought to have diverged around 380 million years ago (Misof et al. 2014). We also compared the Para sequence from *Schistocerca* to other Polyneopteran species focusing on the *Drosophila* optional exons j, i, a, b, e, f and h, which all reside in intracellular loops and whose sequences are thought to

play a role in NaV channel modulation (Lin et al. 2009; Dong et al. 2014). We found no evidence for exon f in any of the Polyneopterans we examined. Conversely, exons i, a and h were present in all isoforms and thus do not appear to be optional. Among splice variants in intracellular loops, only exons a and b are highly conserved with *Drosophila*, consistent with the fact that their sequences are thought to play a role in protein kinase mediated phosphorylation and modulation of the channel (Dong et al. 2014). With respect to the mutually exclusive exons in *Drosophila*, c/d and k/L, which encode parts of two transmembrane domains in Domain II and III of the channel, we found no evidence of a d variant in any of the Polyneopteran species. One other sequence that is highly conserved in the intracellular loops of the protein is the sequence targeted by the pan-Nav antibody. This sequence is also highly conserved across vertebrate NaV channels, conferring to the antibody its broad staining spectrum. Antibodies against this segment were shown to slow down the inactivation of NaV channels (Vassilev et al. 1988). This segment has been proposed to move along with the 'IFM' segment to block the channel during inactivation according to a 'hinged-lid' model (Kellenberger et al. 1997a, b; Catterall 2000; Pan et al. 2018). Notably, our results reveal that this sequence is also highly conserved in insects, explaining the staining observed in *Schistocerca* and *Drosophila*. Conservation across humans, grasshoppers and vinegar flies is consistent with an important role in NaV channel inactivation and opens the possibility that pan-Nav will be effective against NaV channels in a broad range of invertebrate species.

In summary, while much remains to be learned about how NaV channels influence visual processing in the context of collision avoidance behaviors and in olfactory processing, our results highlight the important role and broad localization of NaV channels in the grasshopper and vinegar fly brain as well as their relationship with homologous insect and vertebrate channels.

**Acknowledgements** Stocks obtained from the Bloomington Drosophila Stock Center (NIH P40OD018537) were used in this study. This research was supported by NIH MH-065339, NIH GM-109938, NSF IIS-1607518, and NSF IOS-1253493. The authors would like to thank Dr. M. Rasband for suggesting the use of the pan-Nav antibody, providing a generous supply of it, and helping with the design and interpretation of early experiments using it. Additionally, the authors would like to thank Dr. Y. Zhu for technical assistance and Drs. E. Cooper and M. Rasband for comments on the manuscript.

## References

Afgan E, Baker D, Batut B, van den Beek M, Bouvier D, Čech M, Chilton J, Clements D, Coraor N, Grüning BA, Guerler A, Hillman-Jackson J, Hiltemann S, Jalili V, Rasche H, Soranzo N, Goecks J, Taylor J, Nekrutenko A, Blankenberg D (2018) The Galaxy platform for accessible, reproducible and collaborative biomedical analyses: 2018 update. Nucleic Acids Res 46:W537–W544. https://doi.org/10.1093/nar/gky379

Amichot M, Castella C, Bergé JB, Pauron D (1993) Transcription analysis of the *para* gene by in situ hybridization and immunological characterization of its expression product in wild-type and mutant strains of *Drosophila*. Insect Biochem Mol Biol 23:381–390

Blankenberg D, Gordon A, Von Kuster G, Coraor N, Taylor J, Nekrutenko A, Team G (2010) Manipulation of FASTQ data with Galaxy. Bioinformatics 26:1783–1785. https://doi.org/10.1093/bioinformatics/btq281

Bolger AM, Lohse M, Usadel B (2014) Trimmomatic: a flexible trimmer for Illumina sequence data. Bioinformatics 30:2114–2120. https://doi.org/10.1093/bioinformatics/btu170

Capes DL, Goldschen-Ohm MP, Arcisio-Miranda M, Bezanilla F, Chanda B (2013) Domain IV voltage-sensor movement is both sufficient and rate limiting for fast inactivation in sodium channels. J Gen Physiol 142:101–112. https://doi.org/10.1085/jgp.201310998

Capinera JL (1993) Differentiation of nymphal instars in *Schistocerca americana* (Orthoptera: Acrididae). Fla Entomol 76:175–179. https://doi.org/10.2307/3496026

Catterall WA (2000) From ionic currents to molecular mechanisms: the structure and function of voltage-gated sodium channels. Neuron 26:13–25. https://doi.org/10.1016/S0896-6273(00)81133-2

Chiamvimonvat N, Pérez-García MT, Tomaselli GF, Marban E (1996) Control of ion flux and selectivity by negatively charged residues in the outer mouth of rat sodium channels. J Physiol 491(Pt 1):51–59

Clairfeuille T, Cloake A, Infield DT, Llongueras JP, Arthur CP, Rong Li Z, Jian Y, Martin-Eauclaire M-F, Bougis PE, Ciferri C, Ahern CA, Bosmans F, Hackos DH, Rohou A, Payandeh J (2019) Structural basis of α-scorpion toxin action on $Na_v$ channels. Science 363:eaav8573. https://doi.org/10.1126/science.aav8573

Cuntz H, Haag J, Borst A (2003) Neural image processing by dendritic networks. Proc Natl Acad Sci USA 100:11082–11085. https://doi.org/10.1073/pnas.1830705100

Dapson R (2007) Macromolecular changes caused by formalin fixation and antigen retrieval. Biotech Histochem 82:133–140. https://doi.org/10.1080/10520290701567916

Dapson RW (2010) Mechanisms of action and proper use of common fixatives. In: Shi S-R, Taylor CR (eds) Antigen retrieval immunohistochemistry based research and diagnostics. Wiley, Hoboken, pp 195–217

Davies TGE, Field LM, Usherwood PNR, Williamson MS (2007) A comparative study of voltage-gated sodium channels in the insecta: implications for pyrethroid resistance in Anopheline and other Neopteran species. Insect Mol Biol 16:361–375. https://doi.org/10.1111/j.1365-2583.2007.00733.x

de Vries SEJ, Clandinin TR (2012) Loom-sensitive neurons link computation to action in the *Drosophila* visual system. Curr Biol 22:353–362. https://doi.org/10.1016/j.cub.2012.01.007

Dewell RB, Gabbiani F (2018) Biophysics of object segmentation in a collision-detecting neuron. eLife 7:e34238

Dewell RB, Gabbiani F (2019) Active membrane conductances and morphology of a collision detection neuron broaden its impedance profile and improve discrimination of input synchrony. J Neurophysiol 122:691–706. https://doi.org/10.1152/jn.00048.2019

Dong K (1997) A single amino acid change in the para sodium channel protein is associated with knockdown-resistance (*kdr*) to pyrethroid insecticides in German cockroach. Insect Biochem Mol Biol 27:93–100. https://doi.org/10.1016/S0965-1748(96)00082-3

Dong K, Du Y, Rinkevich F, Nomura Y, Xu P, Wang L, Silver K, Zhorov BS (2014) Molecular biology of insect sodium channels and pyrethroid resistance. Insect Biochem Mol Biol 50:1–17. https://doi.org/10.1016/j.ibmb.2014.03.012

El Jundi B, Heinze S, Lenschow C, Kurylas A, Rohlfing T, Homberg U (2010) The locust standard brain: a 3D standard of the central complex as a platform for neural network analysis. Front Syst Neurosci 3(3):21. https://doi.org/10.3389/neuro.06.021.2009

Escobar MD, Hunt JL (2017) A cost-effective RNA extraction technique from animal cells and tissue using silica columns. J Biol Methods 4:e72

Feldman DE (2012) The spike-timing dependence of plasticity. Neuron 75:556–571. https://doi.org/10.1016/j.neuron.2012.08.001

Fotowat H, Gabbiani F (2011) Collision detection as a model for sensory-motor integration. Annu Rev Neurosci 34:1–19. https://doi.org/10.1146/annurev-neuro-061010-113632

Fotowat H, Harrison RR, Gabbiani F (2011) Multiplexing of motor information in the discharge of a collision detecting neuron during escape behaviors. Neuron 69:147–158. https://doi.org/10.1016/j.neuron.2010.12.007

Fu L, Niu B, Zhu Z, Wu S, Li W (2012) CD-HIT: accelerated for clustering the next-generation sequencing data. Bioinformatics 28:3150–3152. https://doi.org/10.1093/bioinformatics/bts565

Gnerer JP, Venken KJT, Dierick HA (2015) Gene-specific cell labeling using MiMIC transposons. Nucleic Acids Res 43:e56. https://doi.org/10.1093/nar/gkv113

Gong B, Rhodes KJ, Bekele-Arcuri Z, Trimmer JS (1999) Type I and type II $Na^+$ channel α-subunit polypeptides exhibit distinct spatial and temporal patterning, and association with auxiliary subunits in rat brain. J Comp Neurol 412:342–352. https://doi.org/10.1002/(SICI)1096-9861(19990920)412:2%3c342:AID-CNE11%3e3.0.CO;2-2

Gordon D, Merrick D, Wollner DA, Catterall WA (1988) Biochemical properties of sodium channels in a wide range of excitable tissues studied with site-directed antibodies. Biochemistry 27:7032–7038

Gotham S, Song H (2013) Non-swarming grasshoppers exhibit density-dependent phenotypic plasticity reminiscent of swarming locusts. J Insect Physiol 59:1151–1159. https://doi.org/10.1016/j.jinsphys.2013.08.017

Grabherr MG, Haas BJ, Yassour M, Levin JZ, Thompson DA, Amit I, Adiconis X, Fan L, Raychowdhury R, Zeng Q, Chen Z, Mauceli E, Hacohen N, Gnirke A, Rhind N, di Palma F, Birren BW, Nusbaum C, Lindblad-Toh K, Friedman N, Regev A (2011) Full-length transcriptome assembly from RNA-Seq data without a reference genome. Nat Biotechnol 29:644–652. https://doi.org/10.1038/nbt.1883

Günay C, Sieling FH, Dharmar L, Lin W-H, Wolfram V, Marley R, Baines RA, Prinz AA (2015) Distal spike initiation zone location estimation by morphological simulation of ionic current filtering demonstrated in a novel model of an identified *Drosophila* motoneuron. PLoS Comput Biol 11:e1004189. https://doi.org/10.1371/journal.pcbi.1004189

Harrison MC, Jongepier E, Robertson HM, Arning N, Bitard-Feildel T, Chao H, Childers CP, Dinh H, Doddapaneni H, Dugan S, Gowin J, Greiner HY, Hu H, Hughes DST, Huylmans A-K, Kemena C, Kremer LPM, Lee SL, Lopez-Ezquerra A, Mallet L, Monroy-Kuhn JM, Moser A, Murali SC, Muzny DM, Otani S, Piulachs M-D, Poelchau M, Qu J, Schaub F, Wada-Katsumata A, Worley KC, Xie Q, Ylla G, Poulsen M, Gibbs RA, Schal C, Richards S, Belles X, Korb J, Bornberg-Bauer E (2018) Hemimetabolous genomes reveal molecular basis of termite eusociality. Nat Ecol Evol 2:557–566. https://doi.org/10.1038/s41559-017-0459-1

Hedstrom KL, Xu X, Ogawa Y, Frischknecht R, Seidenbecher CI, Shrager P, Rasband MN (2007) Neurofascin assembles a specialized extracellular matrix at the axon initial segment. J Cell Biol 178:875–886. https://doi.org/10.1083/jcb.200705119

Heinemann SH, Terlau H, Stühmer W, Imoto K, Numa S (1992) Calcium channel characteristics conferred on the sodium channel by single mutations. Nature 356:441. https://doi.org/10.1038/356441a0

Henry MA, Luo S, Levinson SR (2012) Unmyelinated nerve fibers in the human dental pulp express markers for myelinated fibers and show sodium channel accumulations. BMC Neurosci 13:29. https://doi.org/10.1186/1471-2202-13-29

Hong CS, Ganetzky B (1994) Spatial and temporal expression patterns of two sodium channel genes in *Drosophila*. J Neurosci 14:5160–5169. https://doi.org/10.1523/JNEUROSCI.14-09-05160.1994

Hu W, Wang T, Wang X, Han J (2015) $I_h$ channels control feedback regulation from amacrine cells to photoreceptors. PLoS Biol 13:e1002115. https://doi.org/10.1371/journal.pbio.1002115

Imbeaud S, Graudens E, Boulanger V, Barlet X, Zaborski P, Eveno E, Mueller O, Schroeder A, Auffray C (2005) Towards standardization of RNA quality assessment using user-independent classifiers of microcapillary electrophoresis traces. Nucleic Acids Res 33:e56. https://doi.org/10.1093/nar/gni054

Ito K, Shinomiya K, Ito M, Armstrong JD, Boyan G, Hartenstein V, Harzsch S, Heisenberg M, Homberg U, Jenett A, Keshishian H, Restifo LL, Rössler W, Simpson JH, Strausfeld NJ, Strauss R, Vosshall LB (2014) A systematic nomenclature for the insect brain. Neuron 81:755–765. https://doi.org/10.1016/j.neuron.2013.12.017

Jenett A, Rubin GM, Ngo T-TB, Shepherd D, Murphy C, Dionne H, Pfeiffer BD, Cavallaro A, Hall D, Jeter J, Iyer N, Fetter D, Hausenfluck JH, Peng H, Trautman ET, Svirskas RR, Myers EW, Iwinski ZR, Aso Y, DePasquale GM, Enos A, Hulamm P, Chun Benny Lam S, Li H-H, Laverty TR, Long F, Qu L, Murphy SD, Rokicki K, Safford T, Shaw K, Simpson JH, Sowell A, Tae S, Yu Y, Zugates CT (2012) A GAL4-driver line resource for *Drosophila* neurobiology. Cell Rep 2:991–1001. https://doi.org/10.1016/j.celrep.2012.09.011

Jortner RA, Farivar SS, Laurent G (2007) A simple connectivity scheme for sparse coding in an olfactory system. J Neurosci 27:1659–1669. https://doi.org/10.1523/JNEUROSCI.4171-06.2007

Kellenberger S, West JW, Catterall WA, Scheuer T (1997a) Molecular analysis of potential hinge residues in the inactivation gate of brain type IIA $Na^+$ channels. J Gen Physiol 109:607–617. https://doi.org/10.1085/jgp.109.5.607

Kellenberger S, West JW, Scheuer T, Catterall WA (1997b) Molecular analysis of the putative inactivation particle in the inactivation gate of brain Type IIA $Na^+$ channels. J Gen Physiol 109:589–605. https://doi.org/10.1085/jgp.109.5.589

Krapp HG, Hengstenberg R (1996) Estimation of self-motion by optic flow processing in single visual interneurons. Nature 384:463–466

Kuehn C, Duch C (2013) Putative excitatory and putative inhibitory inputs are localised in different dendritic domains in a *Drosophila* flight motoneuron. Eur J Neurosci 37:860–875. https://doi.org/10.1111/ejn.12104

Kuitert LC, Connin RV (1952) Biology of the American grasshopper in the southeastern United States. Fla Entomol 35:22–33. https://doi.org/10.2307/3492928

Kurylas AE, Rohlfing T, Krofczik S, Jenett A, Homberg U (2008) Standardized atlas of the brain of the desert locust, *Schistocerca gregaria*. Cell Tissue Res 333:125–145. https://doi.org/10.1007/s00441-008-0620-x

Langmead B, Salzberg SL (2012) Fast gapped-read alignment with Bowtie 2. Nat Methods 9:357–359. https://doi.org/10.1038/nmeth.1923

Langmead B, Trapnell C, Pop M, Salzberg SL (2009) Ultrafast and memory-efficient alignment of short DNA sequences to the human genome. Genome Biol 10:R25. https://doi.org/10.1186/gb-2009-10-3-r25

Li H (2011a) Improving SNP discovery by base alignment quality. Bioinformatics 27:1157–1158. https://doi.org/10.1093/bioinformatics/btr076

Li H (2011b) A statistical framework for SNP calling, mutation discovery, association mapping and population genetical parameter estimation from sequencing data. Bioinformatics 27:2987–2993. https://doi.org/10.1093/bioinformatics/btr509

Li W, Godzik A (2006) Cd-hit: a fast program for clustering and comparing large sets of protein or nucleotide sequences. Bioinformatics 22:1658–1659. https://doi.org/10.1093/bioinformatics/btl158

Li H, Handsaker B, Wysoker A, Fennell T, Ruan J, Homer N, Marth G, Abecasis G, Durbin R, 1000 Genome Project Data Processing Subgroup (2009) The Sequence alignment/map format and SAMtools. Bioinformatics 25:2078–2079. https://doi.org/10.1093/bioinformatics/btp352

Lin W-H, Wright DE, Muraro NI, Baines RA (2009) Alternative splicing in the voltage-gated sodium channel DmNa$_v$ regulates activation, inactivation, and persistent current. J Neurophysiol 102:1994–2006. https://doi.org/10.1152/jn.00613.2009

Lorincz A, Nusser Z (2008) Specificity of immunoreactions: the importance of testing specificity in each method. J Neurosci 28:9083–9086. https://doi.org/10.1523/JNEUROSCI.2494-08.2008

Lorincz A, Nusser Z (2010) Molecular identity of dendritic voltage-gated sodium channels. Science 328:906–909. https://doi.org/10.1126/science.1187958

Loughney K, Kreber R, Ganetzky B (1989) Molecular analysis of the *para* locus, a sodium channel gene in *Drosophila*. Cell 58:1143–1154. https://doi.org/10.1016/0092-8674(89)90512-6

Macharia RW, Ombura FL, Aroko EO (2015) Insects' RNA profiling reveals absence of "hidden break" in 28S ribosomal RNA molecule of onion thrips *Thrips tabaci*. J Nucleic Acids 2015:965294. https://doi.org/10.1155/2015/965294

MacLeod K, Bäcker A, Laurent G (1998) Who reads temporal information contained across synchronized and oscillatory spike trains? Nature 395:693–698. https://doi.org/10.1038/27201

Maisak MS, Haag J, Ammer G, Serbe E, Meier M, Leonhardt A, Schilling T, Bahl A, Rubin GM, Nern A, Dickson BJ, Reiff DF, Hopp E, Borst A (2013) A directional tuning map of *Drosophila* elementary motion detectors. Nature 500:212–216. https://doi.org/10.1038/nature12320

Misof B, Liu S, Meusemann K, Peters RS, Donath A, Mayer C, Frandsen PB, Ware J, Flouri T, Beutel RG, Niehuis O, Petersen M, Izquierdo-Carrasco F, Wappler T, Rust J, Aberer AJ, Aspöck U, Aspöck H, Bartel D, Blanke A, Berger S, Böhm A, Buckley TR, Calcott B, Chen J, Friedrich F, Fukui M, Fujita M, Greve C, Grobe P, Gu S, Huang Y, Jermiin LS, Kawahara AY, Krogmann L, Kubiak M, Lanfear R, Letsch H, Li Y, Li Z, Li J, Lu H, Machida R, Mashimo Y, Kapli P, McKenna DD, Meng G, Nakagaki Y, Navarrete-Heredia JL, Ott M, Ou Y, Pass G, Podsiadlowski L, Pohl H, von Reumont BM, Schütte K, Sekiya K, Shimizu S, Slipinski A, Stamatakis A, Song W, Su X, Szucsich NU, Tan M, Tan X, Tang M, Tang J, Timelthaler G, Tomizuka S, Trautwein M, Tong X, Uchifune T, Walzl MG, Wiegmann BM, Wilbrandt J, Wipfler B, Wong TKF, Wu Q, Wu G, Xie Y, Yang S, Yang Q, Yeates DK, Yoshizawa K, Zhang Q, Zhang R, Zhang W, Zhang Y, Zhao J, Zhou C, Zhou L, Ziesmann T, Zou S, Li Y, Xu X, Zhang Y, Yang H, Wang J, Wang J, Kjer KM, Zhou X (2014) Phylogenomics resolves the timing and pattern of insect evolution. Science 346:763–767. https://doi.org/10.1126/science.1257570

Miyazaki M, Ohyama K, Dunlap DY, Matsnmura F (1996) Cloning and sequencing of the *para*-type sodium channel gene from susceptible and *kdr*-resistant German cockroaches (*Blattella germanica*) and house fly (*Musca domestica*). Mol Gen Genet 252:61–68

Moignot B, Lemaire C, Quinchard S, Lapied B, Legros C (2009) The discovery of a novel sodium channel in the cockroach *Periplaneta americana*: evidence for an early duplication of the *para*-like gene. Insect Biochem Mol Biol 39:814–823. https://doi.org/10.1016/j.ibmb.2009.09.006

Moran Y, Barzilai MG, Liebeskind BJ, Zakon HH (2015) Evolution of voltage-gated ion channels at the emergence of Metazoa. J Exp Biol 218:515–525. https://doi.org/10.1242/jeb.110270

O'Shea M (1975) Two sites of axonal spike initiation in a bimodal interneuron. Brain Res 96:93–98

Ott SR (2008) Confocal microscopy in large insect brains: Zinc–formaldehyde fixation improves synapsin immunostaining and preservation of morphology in whole-mounts. J Neurosci Methods 172:220–230. https://doi.org/10.1016/j.jneumeth.2008.04.031

Pan X, Li Z, Zhou Q, Shen H, Wu K, Huang X, Chen J, Zhang J, Zhu X, Lei J, Xiong W, Gong H, Xiao B, Yan N (2018) Structure of the human voltage-gated sodium channel Na$_v$1.4 in complex with β1. Science 362:305. https://doi.org/10.1126/science.aau2486

Peek MY, Card GM (2016) Comparative approaches to escape. Curr Opin Neurobiol 41:167–173. https://doi.org/10.1016/j.conb.2016.09.012

Peng H, Ruan Z, Long F, Simpson JH, Myers EW (2010) V3D enables real-time 3D visualization and quantitative analysis of large-scale biological image data sets. Nat Biotechnol 28:348–353. https://doi.org/10.1038/nbt.1612

Perez-Orive J, Mazor O, Turner GC, Cassenaer S, Wilson RI, Laurent G (2002) Oscillations and sparsening of odor representations in the mushroom body. Science 297:359–365. https://doi.org/10.1126/science.1070502

Peron S, Gabbiani F (2009) Spike frequency adaptation mediates looming stimulus selectivity in a collision-detecting neuron. Nat Neurosci 12:318–326. https://doi.org/10.1038/nn.2259

Pfeiffer BD, Jenett A, Hammonds AS, Ngo T-TB, Misra S, Murphy C, Scully A, Carlson JW, Wan KH, Laverty TR, Mungall C, Svirskas R, Kadonaga JT, Doe CQ, Eisen MB, Celniker SE, Rubin GM (2008) Tools for neuroanatomy and neurogenetics in *Drosophila*. Proc Natl Acad Sci USA 105:9715–9720. https://doi.org/10.1073/pnas.0803697105

Pfeiffer BD, Truman JW, Rubin GM (2012) Using translational enhancers to increase transgene expression in *Drosophila*. Proc Natl Acad Sci USA 109:6626–6631. https://doi.org/10.1073/pnas.1204520109

Ramos-Vara JA, Miller MA (2014) When tissue antigens and antibodies get along: revisiting the technical aspects of immunohistochemistry—the red, brown, and blue technique. Vet Pathol 51:42–87. https://doi.org/10.1177/0300985813505879

Rasband MN, Peles E, Trimmer JS, Levinson RS, Lux SE, Shrager P (1999) Dependence of nodal sodium channel clustering on paranodal axoglial contact in the developing CNS. J Neurosci 19:7516–7528. https://doi.org/10.1523/JNEUROSCI.19-17-07516.1999

Redondo BB, Bunz M, Halder P, Sadanandappa MK, Mühlbauer B, Erwin F, Hofbauer A, Rodrigues V, VijayRaghavan K, Ramaswami M, Rieger D, Wegener C, Förster C, Buchner E (2013) Identification and structural characterization of interneurons of the *Drosophila* brain by monoclonal antibodies of the Würzburg hybridoma library. PLoS ONE 8:e75420. https://doi.org/10.1371/journal.pone.0075420

Rhodes KJ, Trimmer JS (2006) Antibodies as valuable neuroscience research tools versus reagents of mass distraction. J Neurosci 26:8017–8020. https://doi.org/10.1523/JNEUROSCI.2728-06.2006

Saha D, Leong K, Li C, Peterson S, Siegel G, Raman B (2013) A spatiotemporal coding mechanism for background-invariant odor recognition. Nat Neurosci 16:1830–1839. https://doi.org/10.1038/nn.3570

Shao Y-M, Dong K, Tang Z-H, Zhang C-X (2009) Molecular characterization of a sodium channel gene from the Silkworm *Bombyx mori*. Insect Biochem Mol Biol 39:145–151. https://doi.org/10.1016/j.ibmb.2008.10.005

Simão FA, Waterhouse RM, Ioannidis P, Kriventseva EV, Zdobnov EM (2015) BUSCO: assessing genome assembly and annotation completeness with single-copy orthologs. Bioinformatics 31:3210–3212. https://doi.org/10.1093/bioinformatics/btv351

Simmons PJ, Sztarker J, Rind FC (2013) Looming detection by identified visual interneurons during larval development of the locust *Locusta migratoria*. J Exp Biol 216:2266–2275. https://doi.org/10.1242/jeb.083360

Simões P, Ott SR, Niven JE (2011) Associative olfactory learning in the desert locust, *Schistocerca gregaria*. J Exp Biol 214:2495–2503. https://doi.org/10.1242/jeb.055806

Smith-Unna R, Boursnell C, Patro R, Hibberd JM, Kelly S (2016) TransRate: reference-free quality assessment of de novo transcriptome assemblies. Genome Res 26:1134–1144. https://doi.org/10.1101/gr.196469.115

Soderlund DM (2005) 5.1 - Sodium channels. In: Gilbert LI (ed) Comprehensive molecular insect science. Elsevier, Amsterdam, pp 1–24

Srinivasan MV, Laughlin SB, Dubs A, Horridge GA (1982) Predictive coding: a fresh view of inhibition in the retina. Proc R Soc Lond B Biol Sci 216:427–459. https://doi.org/10.1098/rspb.1982.0085

Strausfeld NJ (1976) Atlas of an insect brain. Springer Verlag, Berlin, Heidelberg

Strausfeld NJ (2009) Brain organization and the origin of insects: an assessment. Proc R Soc Lond B Biol Sci 276:1929–1937. https://doi.org/10.1098/rspb.2008.1471

Su Y-Y, Ye M, Li L, Liu C, Pan J, Liu W-W, Jiang Y, Jiang X-Y, Zhang X, Shu Y, Bao L (2013) KIF5B promotes the forward transport and axonal function of the voltage-gated sodium channel $Na_v1.8$. J Neurosci 33:17884–17896. https://doi.org/10.1523/JNEUROSCI.0539-13.2013

Suzuki T, Yamato S (2018) Mode of action of piperovatine, an insecticidal piperamide isolated from *Piper piscatorum* (Piperaceae), against voltage-gated sodium channels. Neurotoxicology 69:288–295. https://doi.org/10.1016/j.neuro.2018.07.021

Sztarker J, Rind FC (2014) A look into the cockpit of the developing locust: looming detectors and predator avoidance. Dev Neurobiol 74:1078–1095. https://doi.org/10.1002/dneu.22184

Terlau H, Heinemann SH, Stühmer W, Pusch M, Conti F, Imoto K, Numa S (1991) Mapping the site of block by tetrodotoxin and saxitoxin of sodium channel II. FEBS Lett 293:93–96

Terrapon N, Li C, Robertson HM, Ji L, Meng X, Booth W, Chen Z, Childers CP, Glastad KM, Gokhale K, Gowin J, Gronenberg W, Hermansen RA, Hu H, Hunt BG, Huylmans AK, Khalil SMS, Mitchell RD, Munoz-Torres MC, Mustard JA, Pan H, Reese JT, Scharf ME, Sun F, Vogel H, Xiao J, Yang W, Yang Z, Yang Z, Zhou J, Zhu J, Brent CS, Elsik CG, Goodisman MAD, Liberles DA, Roe RM, Vargo EL, Vilcinskas A, Wang J, Bornberg-Bauer E, Korb J, Zhang G, Liebig J (2014) Molecular traces of alternative social organization in a termite genome. Nat Commun 5:3636. https://doi.org/10.1038/ncomms4636

Thackeray JR, Ganetzky B (1994) Developmentally regulated alternative splicing generates a complex array of *Drosophila para* sodium channel isoforms. J Neurosci 14:2569–2578. https://doi.org/10.1523/jneurosci.14-05-02569.1994

Thurber GM, Schmidt MM, Wittrup KD (2008) Antibody tumor penetration: transport opposed by systemic and antigen-mediated clearance. Adv Drug Deliv Rev 60:1421–1434. https://doi.org/10.1016/j.addr.2008.04.012

Thurmond J, Goodman JL, Strelets VB, Attrill H, Gramates LS, Marygold SJ, Matthews BB, Millburn G, Antonazzo G, Trovisco V, Kaufman TC, Calvi BR, FlyBase Consortium (2019) FlyBase 2.0: the next generation. Nucleic Acids Res 47:D759–D765. https://doi.org/10.1093/nar/gky1003

Trunova S, Baek B, Giniger E (2011) Cdk5 regulates the size of an axon initial segment-like compartment in mushroom body neurons of the *Drosophila* central brain. J Neurosci 31:10451–10462. https://doi.org/10.1523/JNEUROSCI.0117-11.2011

van Hateren JH (1992) Theoretical predictions of spatiotemporal receptive fields of fly LMCs, and experimental validation. J Comp Physiol A 171:157–170. https://doi.org/10.1007/BF00188924

Vassilev PM, Scheuer T, Catterall WA (1988) Identification of an intracellular peptide segment involved in sodium channel inactivation. Science 241:1658–1661. https://doi.org/10.1126/science.2458625

Venken KJT, Schulze KL, Haelterman NA, Pan H, He Y, Evans-Holm M, Carlson JW, Levis RW, Spradling AC, Hoskins RA, Bellen HJ (2011) MiMIC: a highly versatile transposon insertion resource for engineering *Drosophila melanogaster* genes. Nat Methods 8:737–743

von Reyn CR, Breads P, Peek MY, Zhiyu Zheng G, Williamson WR, Yee AL, Leonardo A, Card GM (2014) A spike-timing mechanism for action selection. Nat Neurosci 17:962–970. https://doi.org/10.1038/nn.3741

West JW, Patton DE, Scheuer T, Wang Y, Goldin AL, Catterall WA (1992) A cluster of hydrophobic amino acid residues required for fast $Na^+$-channel inactivation. Proc Natl Acad Sci USA 89:10910–10914

Wingett SW, Andrews S (2018) FastQ screen: a tool for multi-genome mapping and quality control. F1000Res 7:1338. https://doi.org/10.1288/f1000research.15931.2

Winnebeck EC, Millar CD, Warman GR (2010) Why does insect RNA look degraded? J Insect Sci 10:159. https://doi.org/10.1673/031.010.14119

Wipfler B, Letsch H, Frandsen PB, Kaplif P, Mayerh C, Barteli D, Buckley TR, Donath A, Edgerly-Rooks JS, Fujita M, Liu S, Machida R, Mashimo Y, Misof B, Niehuis O, Peters RS, Petersen M, Podsiadlowski L, Schütte K, Shimizu S, Uchifune T, Wilbrandt J, Yan E, Zhou X, Simon S (2019) Evolutionary history of *Polyneoptera* and its implications for our understanding of early winged insects. Proc Natl Acad Sci USA 116:3024–3029. https://doi.org/10.1073/pnas.1817794116

Wu JS, Luo L (2006) A protocol for dissecting *Drosophila melanogaster* brains for live imaging or immunostaining. Nat Protoc 1:2110–2115. https://doi.org/10.1038/nprot.2006.336

Wu M, Nern A, Williamson WR, Morimoto MM, Reiser MB, Card GM, Rubin GM (2016) Visual projection neurons in the *Drosophila* lobula link feature detection to distinct behavioral programs. eLife 5:e21022. https://doi.org/10.7554/eLife.21022

Xiao X, Chen C, Yu T-M, Ou J, Rui M, Zhai Y, He Y, Xue L, Ho MS (2017) Molecular chaperone calnexin regulates the function of *Drosophila* sodium channel Paralytic. Front Mol Neurosci 10:57. https://doi.org/10.3389/fnmol.2017.00057

Zhu Y, Gabbiani F (2018) Combined two-photon calcium imaging and single-ommatidium visual stimulation to study fine-scale retinotopy in insects. Extracellular recording approaches. Springer, Berlin, pp 185–206